Targeting Oxidative Phosphorylation with a Mitochondrial Complex I Inhibitor is limited by Mechanism-based Toxicity

Marina Konopleva (mkonople@mdanderson.org)
The University of Texas MD Anderson Cancer Center https://orcid.org/0000-0002-9347-2212
Timothy Yap
The University of Texas MD Anderson Cancer Center https://orcid.org/0000-0002-2154-3309
Naval Daver
The University of Texas MD Anderson Cancer Center
Mikhila Mahendra
University of Texas MD Anderson Cancer Center
Jixiang Zhang
The University of Texas MD Anderson Cancer Center https://orcid.org/0000-0002-1641-8650
Carlos Kamiya-Matsuoka
The University of Texas MD Anderson Cancer Center
Funda Meric-Bernstam
MD Anderson Cancer Center https://orcid.org/0000-0001-6816-6072
Hagop Kantarjian
The University of Texas MD Anderson Cancer Center https://orcid.org/0000-0002-1908-3307
Farhad Ravandi
University of Texas - M.D. Anderson Cancer Center https://orcid.org/0000-0002-7621-377X
Meghan Collins
The University of Texas at Austin
Maria Di Francesco
The University of Texas MD Anderson Cancer Center
Ecaterina Dumbrava
The University of Texas MD Anderson Cancer Center
Siqing Fu
UT MD Anderson Cancer Center https://orcid.org/0000-0002-1933-0419
Sisi Gao
The University of Texas MD Anderson Cancer Center
Jason Gay
University of Texas MD Anderson Cancer Center
Sonal Gera

The University of Texas MD Anderson Cancer Center

Jing Han
University of Texas MD Anderson Cancer Center

David Hong
The University of Texas MD Anderson Cancer Center

Elias Jabbour
The University of Texas MD Anderson Cancer Center

Zhenlin Ju
The University of Texas MD Anderson Cancer Center

Daniel Karp
The University of Texas MD Anderson Cancer Center

Alessia Lodi
The University of Texas at Austin

Jennifer Molina
University of Texas MD Anderson Cancer Center

Natalia Baran
The University of Texas MD Anderson Cancer Center https://orcid.org/0000-0003-0618-4798

Aung Naing
The University of Texas MD Anderson Cancer Center https://orcid.org/0000-0002-4803-8513

Maro Ohanian
The University of Texas MD Anderson Cancer Center

Shubham Pant
The University of Texas MD Anderson Cancer Center

Naveen Pemmaraju
MD Anderson

Prithviraj Bose
The University of Texas MD Anderson Cancer Center https://orcid.org/0000-0002-4343-5712

Sarina A. Piha-Paul
The University of Texas M.D. Anderson Cancer Center

Jordi Rodon
Hospital Universitari Vall d'Hebron

Carolina Salguero
The University of Texas MD Anderson Cancer Center

Koji Sasaki
The University of Texas MD Anderson Cancer Center https://orcid.org/0000-0002-9140-0610

Anand Singh
The University of Texas MD Anderson Cancer Center

Vivek Subbiah
The University of Texas MD Anderson Cancer Center https://orcid.org/0000-0002-6064-6837

Apostolia M. Tsimberidou
The University of Texas MD Anderson Cancer Center
Quanyun Xu
University of Texas MD Anderson Cancer Center
Musa Yilmaz
The University of Texas MD Anderson Cancer Center
Qi Zhang
University of Texas M.D. Anderson Cancer Center https://orcid.org/0000-0002-7918-8952
Christopher Bristow
University of Texas MD Anderson Cancer Center
Meenakshi Bhattacharjee
UT Health, University of Texas Medical School at Houston
Stefano Tiziani
The University of Texas at Austin
Timothy Heffernan
Translational Research to Advance Therapeutics and Innovation in Oncology (TRACTION), The University of Texas MD Anderson Cancer Center, Houston, TX https://orcid.org/0000-0002-3166-8922
Christopher Vellano
1. Department of Systems Biology, The University of Texas MD Anderson Cancer Center, Houston, TX 77030
Philip Jones
University of Texas MD Anderson Cancer Center
Cobi Heijnen
University of Texas M.D. Anderson Cancer Center
Annemieke Kavelaars
University of Texas M.D. Anderson Cancer Center
Joseph Marszalek
University of Texas MD Anderson Cancer Center

Article

Keywords:

Posted Date: April 6th, 2022

DOI: https://doi.org/10.21203/rs.3.rs-1506700/v1

Version of Record: A version of this preprint was published at Nature Medicine on January 19th, 2023. See the published version at https://doi.org/10.1038/s41591-022-02103-8.

Abstract

While targeting oxidative phosphorylation (OXPHOS) is a rational anticancer strategy, patient benefit with OXPHOS inhibitors in the clinic has yet to be achieved. Based on promising preclinical data, we advanced IACS-010759, a highly potent and selective small-molecule inhibitor of mitochondrial complex I, into two phase I trials in patients with acute myeloid leukemia (NCT02882321) or advanced solid tumors (NCT03291938). Clinical findings revealed that IACS-010759 had a narrow therapeutic index with emergent dose-limiting toxicities that included elevated blood lactate and neurotoxicity, obstructing efforts to maintain target plasma exposure. Consequently, only modest on-target inhibition and limited antitumor activity were observed. Follow-up reverse translational studies uncovered that IACS-010759 reduced oxygen consumption rates in neurons and damaged myelin. Further, IACS-010759-treated mice displayed behaviors indictive of neuropathy, which were minimized with the co-administration of a histone deacetylase 6 inhibitor. Our findings urge caution in the continued development of complex I inhibitors as antitumor agents.

Introduction

Targeting the oxidative phosphorylation (OXPHOS)[1-6] pathway has emerged as an attractive strategy in cancer therapy due to the dependency of certain tumors on this metabolic pathway[5,7-9]. This therapeutic approach, however, has been limited by poor potency (e.g. biguanides[10,11]), off-target pharmacology (e.g. rotenone[12]), a suboptimal pharmacokinetic (PK) profile[13], and dose-limiting toxicities (e.g. oligomycin, BAY 87-2243[5], and ASP4132[14]). Previously, we reported on the preclinical discovery and development of IACS-010759, a highly potent and selective small-molecule complex I inhibitor with favorable attributes for clinical evaluation[15]. Preclinical studies confirmed that IACS-010759 selectively inhibited mitochondrial complex I, the first of five transmembrane complexes of the electronic transport chain (ETC), by binding to the ND1 subunit at the entrance to the quinone binding channel[15,16]. Efficacious doses of IACS-010759 in multiple human xenograft models of OXPHOS-dependent cancers were well-tolerated, with no neurotoxicity observed, as well as induced energetic stress and decreased aspartate production, resulting in reduced cell viability and apoptosis[15]. Consequently, treatment with our compound extended mouse survival[15]. Additionally, IACS-010759 administration increased extracellular lactate levels in responsive tumor cells[15], indicating a compensatory increase in glycolysis, as well as therapeutic opportunities for targeting OXPHOS in glycolysis-deficient tumors.

Based on these strong preclinical findings[15], IACS-010759 was assessed in two independent Phase I clinical trials. The first-in-human study evaluated patients with relapsed/refractory acute myeloid leukemia (AML), a malignancy strongly dependent on OXPHOS[17-19]. The second trial, which leveraged pharmacokinetic data from the AML study to inform on dosing regimens, enrolled patients with advanced solid tumors, with an emphasis on glycolysis-deficient cancers such as those with *ENO1* loss[15] and *SMARCA1* mutations[20]. Results from these two trials revealed that maintaining clinically effective doses of IACS-010759 was challenging at tolerated doses, requiring intermittent dosing schedules and drug

interruptions, the latter necessary to mitigate drug-related toxicities related to elevated blood lactate and neurotoxicity. Consequently, IACS-010759 achieved modest on-target modulation of OXPHOS and limited antitumor activity, and both trials were discontinued. Follow-up reverse translational studies confirmed that clinically achievable plasma exposures were too low to induce therapeutic efficacy, and escalation to efficacious doses resulted in treatment-induced peripheral neuropathy. Co-administration with an HDAC6 inhibitor, however, mitigated pain associated with IACS-010759-induced peripheral neuropathy in mouse models. Overall, our findings reveal significant risks associated with the clinical development of complex I inhibitors.

Results

Study design and objectives

Two independent, single-arm, single-site, Phase I clinical trials (**Extended Data Fig. 1**) were conducted at The University of Texas MD Anderson Cancer Center to determine the safety, tolerability, pharmacokinetics, pharmacodynamics, and antitumor activity of IACS-010759 in 17 adult patients with relapsed/refractory AML (2016, NCT02882321; 'AML trial') and 23 adult patients with advanced solid tumors (2017, NCT03291938; 'Solid Tumor trial'). In addition to preclinical data, clinical and pharmacokinetic data from the AML trial were used to design the dosing schedules of the Solid Tumor trial. Dosing regimens for both trials are described in *Methods* and **Supplementary Table 1**. Patient characteristics are detailed in **Supplementary Table 2, 3.**

Drug-related toxicities in patients with AML and solid tumors

Adverse events were monitored at scheduled timepoints throughout each trial. Treatment-emergent adverse effects (TEAEs) and treatment-related adverse events (TRAEs) were reported in both trials (**Supplementary Tables 4-7**), with toxicities related to elevated blood lactate or neurotoxicity emerging as the most common adverse events. Specifically, common grade 1-2 TRAEs included elevated blood lactate (35% AML; 83% Solid Tumor), lactic acidosis (29% AML), nausea (29 AML, 65% Solid Tumor), vomiting (18% AML, 30% Solid Tumor), and peripheral neuropathy (12% AML, 35% Solid Tumor). Grade ≥3 TRAEs in both trials included elevated blood lactate (53% AML, 4% Solid Tumor), lactic acidosis (24% AML), nausea (9% Solid Tumor), vomiting (13% Solid Tumor), and peripheral neuropathy (6% AML, 4% Solid Tumor). Of note, one Solid Tumor patient developed grade 3 visual impairment. All severe adverse events (SAEs), fatal SAEs, and TRAEs leading to treatment discontinuation are listed in **Supplementary Table 8-11**.

Elevation of blood lactate has been frequently reported upon OXPHOS inhibition[2,14,15,21,22]. Here, 8/16 AML patients who developed increased blood lactate also developed lactic acidosis (47.1%), with 7/8 cases determined as treatment and 4/8 cases reported as Grade ≥3 (**Supplementary Table 4,6**). Further, 20 patients (87%) in the Solid Tumor trial had treatment-related increases in blood lactate, although no lactic acidosis was detected (**Supplementary Table 7**). Increasing plasma levels of IACS-010759 were

associated with increasing plasma lactate, but not with reduction of blood pH **(Extended Data Fig. 2**), and exposures of >8 nM (or 4.5 ng/mL equivalent) of IACS-010759 were associated with increased probability of elevated lactate **(Fig. 1a,b**). No event related to increased lactate was fatal, although elevated blood lactate resulted in treatment discontinuation in one patient in the Solid Tumor trial (**Supplementary Table 11**).

In both trials, neurotoxicity emerged as a prominent TRAE, with peripheral neuropathy as the most common clinical presentation (**Table 1, Supplementary Table 6,7)**. In general, patients experienced worsening myalgia prior to the onset of peripheral neuropathy. Nerve biopsies collected from two Solid Tumor patients with grade 3 neuropathy revealed mixed axonal and demyelinating neuropathy with involvement of the large and small fibers (axons) in one patient, and histology consistent with axonal neuropathy with loss of the large myelinated fibers in the other patient (**Extended Data Fig. 3**). Overall, incidence of peripheral neuropathy increased with dosage and dose frequency (**Table 1**) as well as with duration on trial **(Fig. 1c**), thus preventing further dose and schedule escalation. Recovery from neuropathy varied among patients, but generally occurred very gradually after drug discontinuation. Interestingly, elevated plasma lactate, but not IACS-010759 exposure, was associated with peripheral neuropathy in the Solid Tumor trial **(Fig. 1d,e**). Additionally, prior allogeneic stem cell transplantation (allo-SCT) significantly (p=0.002) increased the risk of developing peripheral neuropathy in patients with AML, while prior cytotoxic chemotherapy (p=0.005) and/or concomitant diagnosis of diabetes mellitus (p=0.043) increased the risk of peripheral neuropathy in patients with Solid Tumors (**Table 1**).

Overall, the frequency and severity of adverse events related to elevated lactate and neurotoxicity contributed to the premature termination of both trials.

Efficacy

Response in the AML trial was assessed per the European LeukemiaNet (ELN) 2017[23], and responses in the Solid Tumor trial were assessed per RECISTv1.1 guidelines[24]. In the AML trial, no patient responded to IACS-01059 treatment. In the Solid Tumor Trial, one Cohort 4 patient with advanced castration-resistant prostate cancer achieved a confirmed RECISTv1.1 partial response and resolution of cancer-related pain, and remained on study for four months (**Fig. 2)**. An additional eight Solid Tumor patients had a best response of RECISTv1.1 stable disease (**Supplementary Table 12**). No RECISTv1.1 stable disease or objective responses were achieved in any of the three patients with solid tumors with *ENO1* loss, nor in the two patients with *SMARCA1* deletions. The overall lack of objective response, coupled with the frequency of adverse events, resulted in the discontinuation of both trials (**Supplementary Table 12,13**).

Pharmacokinetics of IACS-010759

Consistent with preclinical data[15], plasma levels of IACS-010759 in all patients increased in a dose-dependent manner and were characterized by a long terminal half-life of approximately 16 hours (**Fig. 3;**

Supplementary Table 14). Data from previous preclinical[15] and investigational new drug studies using intermittent dosing schedules indicated that a C_{min} of ~20 nM was needed to achieve antitumor activity in patients. In the first two AML cohorts with QD dosing, IACS-010759 accumulated slowly with repeated dosing over the 21-day daily dosing cycle (**Fig. 3a; Extended Data Fig. 4a)**. This dosing schedule enabled plasma levels of IACS-010759 to approach the target efficacious concentration (dotted line, **Fig. 3a**) in AML Cohort 2 patients by the end of the first cycle, but a steady state was not achieved.

Due to the long half-life and slow accumulation of IACS-010759, as well as the emergence of drug-related toxicities in Cohorts 1 and 2 (see *Drug-related toxicities*), the AML trial protocol was amended with revised dosing schedules that included a 7-day induction phase with QD dosing, followed by a maintenance phase with IACS-010759 given either once (Cohort 3) or three times (Cohort 4) per week (**Extended Data Fig. 1, Supplementary Table 1**). Dosing for the Solid Tumor cohorts was designed with a similar 'induction-maintenance' schedule, with an induction phase of QD dosing for 5 or 7 days, followed by a maintenance phase of IACS-010759 given either once (Cohorts 1-3) or twice (Cohorts 4-6) per week (**Extended Data Fig. 1, Supplementary Table 1**). The induction-maintenance dosing strategy enabled most patients in AML Cohorts 3-4 and all patients in the Solid Tumor trial to approach the target efficacious concentration (dotted lines **Fig. 3b-d; Extended Data Fig. 4b-f**) during the induction phase, and accumulation was not observed during the maintenance phase (**Fig. 3b-d, Extended Data Fig. 4b-f)**. In general, dosing 2x or 3x per week maintained plasma IACS-010759 levels better compared to once weekly dosing (**Fig. 3b-d, Extended Data Fig. 4b-f**). Regardless, IACS-010759 levels of ≥20 nM were not maintained with any evaluated dosing schedule. The emergence of drug-related toxicities, which necessitated dosing holidays, further obstructed efforts to maintain high IACS-010759 exposures. Additional pharmacokinetic properties are in listed in **Supplementary Table 14.**

Evidence of target inhibition in AML blasts

To evaluate the biological response of tumor cells to IACS-010759, AML blasts were isolated from patients in the AML trial to identify changes in oxygen consumption rate (OCR), mitochondria load, metabolites, and gene expression that were indicative of OXPHOS inhibition. Baseline and maximal OCR of AML blasts were modulated following IACS-010759 treatment in a manner consistent with preclinical findings[15]. Specifically, at the end of the first 7-day QD dosing (Cohorts 1-2: Day 14; Cohorts 3-4: Day 7), a consistent and significant decrease was found between baseline (p= 0.001; **Fig. 4a)** and maximal (p= 0.003; **Fig. 4b)** OCR compared to pre-treatment OCR. Indeed, a >25% reduction in baseline and maximal OCR was observed in 6/12 and 8/12 patients, respectively (**Fig. 4a,b**). However, among these AML patients, decreases in baseline and maximal OCR were not maintained in 2/6 patients and in 3/8 patients, respectively (**Fig. 4a,b)** – an effect that aligned with reduced plasma exposures due to the intermittent dosing of IACS-010759 during maintenance in AML Cohorts 3 and 4 **(Fig. 3b; Extended Data Fig. 4b)**. Individually, correlations between IACS-010759 exposure and OCR varied (**Extended Data Fig. 5, 6**), with a significant correlation and an R-square value >0.24 between plasma exposure and baseline OCR in 3 patients (**Extended Data Fig. 5a,c,k**), between plasma exposure and maximal OCR in 5 patients

(**Extended Data Fig. 6a,e,h,k,l**), and between plasma exposure and both baseline and maximal OCR in patients 3 and 17 (**Extended Data Fig. 5a,k; Extended Data Fig. 6a,k**). Poor correlation between IACS-010759 plasma exposure and OCR in several patients, including Patient 4 **(Extended Data Fig. 5b, Extended Data Fig. 6b)**, Patient 7 **(Extended Data Fig. 5f, Extended Data Fig. 6f)**, Patient 8 **(Extended Data Fig. 5c, Extended Data Fig. 6c)**, and Patient 11 **(Extended Data Fig. 5g, Extended Data Fig. 6g)**, suggested the presence of a mechanism of resistance to IACS-010759, such as an increase in mitochondria within the blast to compensate for complex I inhibition[25]. To assess this, we performed longitudinal Q-PCR analysis on blasts from IACS-010759-treated AML patients. Our data identified a significant increase in the ratio between mitochondrial (mtDNA) and genomic (gDNA) DNA (p= 0.04) in most patients **(Fig. 4c)**, which strongly suggested rapid adaptation to IACS-010759 treatment.

Next, the relationship between plasma exposure and the biological response of AML blasts to IACS-010759 was determined. To this end, we assessed and compared modulation of OCR by IACS-010759 in blasts collected from three AML patients in Cohort 4 who received the same dosing regimen (**Supplemental Table 1**) yet achieved differential plasma exposure and modulation of baseline OCR. Specifically, Patients 17, 19, and 16 demonstrated relatively strong, mild, or weak drug-induced reductions in baseline OCR, respectively (**Fig. 4d**). Our previous *in vitro* data showed that IACS-010759 altered levels of metabolites related to complex I inhibition and reduced energetic status[15] (**Fig. 4e**). These changes included 1) inhibiting the conversion of nucleoside monophosphates (NMPs) and nucleoside diphosphates (NDPs) to nucleoside triphosphates (NTPs); 2) inhibiting oxidation of the complex I substrate NADH to NAD+; 3) elevating glutamine, which can be shuttled into alternative fuel pathways in lieu of OXPHOS and aspartate synthesis; and 4) elevating levels of glycolytic endpoints. Here, we found that blasts from Patient 17, who achieved the relatively highest plasma exposure, demonstrated the most robust changes in metabolite levels compared to the other two patients. Specifically, in Patient 17, IACS-010759 significantly elevated intracellular levels of NMPs ($p<0.01$) and NDPs ($p<0.01$), while significantly decreasing intracellular levels of NTPs ($p<0.01$) (**Fig. 4f-h**), suggesting a decrease in NTP production. IACS-010759 treatment significantly decreased levels of NAD+ (p= 0.03) as well as increased levels of tryptophan (p= 0.08) and nicotinamide (p= 0.002), two metabolic precursors of NAD+ (**Extended Data Fig. 7a-c**), suggesting a decrease in NADH oxidation. Glutamine levels trended upward (p = 0.08) (**Extended Data Fig. 7d**) while aspartate levels trended downward (p= 0.06) (**Fig. 4i**), consistent with increased investment in alternative fuel pathways and decreased investment in cell growth. Finally, levels of the glycolytic endpoints in AML blasts from Patient 17 were generally elevated, with a significant increase in alanine (p = 0.046; **Extended Data Fig. 7e**) but no change in lactate (**Fig. 4j**) levels, suggesting increased glycolysis upon complex I inhibition. In contrast, in blasts from Patients 19, who experienced lower IACS-010759 plasma exposure than Patient 17, metabolite changes consistent with complex I inhibition and reduced energetic status were moderate. Specifically, IACS-010759 significantly reduced NTP levels but did not affect NMP and NDP levels in manners consistent with complex I inhibition (**Extended Data Fig. 7g**). Although levels of nicotinamide were significantly increased (p = 0.006; **Extended Data Fig. 7b**) and tryptophan trended upward upon IACS-010759 treatment (**Extended Data Fig. 7c**), NAD+ levels significantly increased (p = 0003; **Extended Data Fig. 7a**), suggesting possible complex I

activity. Significantly decreased glutamine (p = 0.02; **Extended Data Fig. 7d**), unaffected aspartate (**Fig. 4i**), unaffected alanine (**Extended Data Fig. 7e**), and significantly increased lactate (p= 0.005; **Fig. 4j**) levels upon IACS-010759 treatment in blasts from Patient 19 suggested no increase in the activation of alternative fuel pathways. Finally, in blasts from Patient 16, who achieved the relatively weakest IACS-010759 plasma exposure, metabolite changes did not indicate impaired complex I activity or reduced energetic status. Specifically, IACS-010759 treatment did not affect levels of NMP, NDP, and NTP (**Extended Data Fig. 7f**) nor levels of NAD+ (**Extended Data Fig. 7a**), nicotinamide (**Extended Data Fig. Fig 7b**), and tryptophan (**Extended Data Fig. Fig 7c**). Levels of glutamine (**Extended Data Fig. Fig 7d**), lactate (**Fig. 4j**), and alanine (**Extended Data Fig. 7e**) were unaffected, and levels of aspartate were significantly elevated (p = 0.02; **Fig. 4i**) upon IACS-010759 treatment, suggesting no increase in the activation of alternative fuel pathways. These findings, along with metabolite data from Patient 19, suggest that AML blasts from Patient 19 and 16 may still obtain energy from the OXPHOS pathway even during IACS-010759 exposure. Overall, our comparison of metabolite data from Patients 17, 19, and 16 suggests that high plasma exposure of IACS-010759 is needed to modulate AML blast biology in a manner that indicates complex I inhibition and low energetic status.

To evaluate the effects of complex I inhibition on gene expression in AML blasts from Patients 16, 17, and 19, we first conducted hierarchical clustering using our previously published nanoString signature generated from preclinical data[15] and a new signature with 1065 mRNAs that were significantly modulated in AML blasts (**Fig. 4k**). Among the 176 genes identified in our previous OXPHOS signature, 166 genes were present in this patient sample RNA-seq dataset, and only 11 genes overlapped with the 1065 genes in the new signature. Quantification of the nanoString gene expression suggests modulation of biology across all samples upon IACS-010759 treatment. Interestingly, unlike treatment-induced modulation of OCR and metabolites (**Fig. 4d, f-j; Extended Data Fig. 7**), modulation of gene expression across both nanoString and newly identified signatures was consistent across all three AML patients. Next, we conducted Gene Ontology (GO) enrichment analysis on RNA-sequencing (RNA-seq) results from AML blasts obtained from these same patients in Cohort 4 pre- and post-dose at various timepoints across Cycle 1. Downregulation of mRNAs related to chromatin organization and DNA damage response, as well as enrichment for terms related to RNA/DNA metabolism and transport, were detected across post-dose samples, including those from Patient 16 (**Extended Data Fig. 8a**). Pathway analysis was then used to detect deregulated biological pathways upon IACS-010759 treatment. Consistent with changes in GO terms, pathways related to tRNA biosynthesis were upregulated while pathways related to cell growth, RTK/PI3K signaling, and proliferation were downregulated upon IACS-010759 treatment (**Extended Data Fig. 8b**). Once again, these changes were detected in all three patients, regardless of plasma exposure (**Extended Data Fig. 8b**). Overall, IACS-010759-induced changes in gene expression align with preclinical findings that show increased DNA damage as well as inhibited nucleotide biosynthesis and cell proliferation upon treatment[15], but do not align with treatment-induced changes in plasma exposure and metabolites.

Our findings suggest that low plasma exposures of IACS-010759 can induce changes in biomarkers and pathways associated with oxidative metabolism in AML blasts, but high plasma exposures are needed to achieve modulation of metabolites in a manner consistent with complex I inhibition. Unfortunately, as indicated by the low response rate, treatment-induced changes in AML blasts were insufficient to reduce disease burden.

Reverse Translational Studies

As previously described (**Fig. 3, Extended Data Fig. 4)**, the target plasma exposure of 20 nM was not maintained in either trial. Further, achieved exposures induced limited antitumor activity (**Fig. 2, Supplementary Table 12**) and elicited high rates of adverse events related to elevated lactate and neurotoxicity (**Table 1, Supplementary Tables 4-11**). Reverse translational studies were thus conducted to investigate the efficacy and toxicities induced by doses aligned with observed clinical exposures of IACS-010759 as well as to evaluate strategies for mitigating complex I-induced toxicities.

First, we performed a pharmacokinetics study assessing 0.1, 0.3, 1 and 5 mg/kg IACS-010759 administered on a 5-days on/2-days off dosing schedule in NSG and C56Bl6 mice. Doses of 0.1 and 0.3 mg/kg generated Cmax exposures that were most similar (20-40 nM) to the highest exposures achieved in AML and Solid Tumor clinical trials (**Fig. 5a**), and, consistent with data from AML blasts, these doses induced intermediate modulation of baseline OCR (**Fig. 5b**). However, doses higher than 0.1 and 0.3 mg/kg were needed to enhance median survival in these models, with only 1 mg/kg or 5 mg/kg of IACS-010759 extending median survival in mice by 7 and 35 days, respectively (**Fig. 5c)**. All doses, including the non-efficacious 0.3 mg/kg dose, elevated plasma lactate in C56Bl6 mice, while only the 5 mg/kg dose elevated plasma lactate elevated plasma lactate in NSG mice (**Extended Data Fig. 9**). Consistent with clinical data, these findings confirm that the clinically achievable IACS-010759 exposures modestly modulate OCR, elevate lactate, and are not efficacious.

To further explore the relationships among IACS-010759 treatment, elevated blood lactate, and neurotoxicity, we investigated this phenotype in C57/Bl6 mice treated with escalating doses of IACS-010759. Mice were treated with IACS-010759 for two weeks with a 5-days on/2-days off dosing schedule. Mechanical allodynia, a behavioral symptom of neuropathy, was measured over time using von Frey hairs[26]. IACS-010759 induced mechanical allodynia in a dose-dependent manner, and it did not resolve by two weeks after the last dose (**Fig. 5d**). To determine if IACS-010759 also induced spontaneous pain, we used a conditioned place preference (CPP) paradigm, in which mice were conditioned to associate the light chamber with retigabine-induced pain relief (**Extended Data Fig. 10a**). Mice treated with IACS-010759 spent significantly more time in the light chamber compared to mice treated with vehicle, indicating treatment-induced spontaneous pain (**Extended Data Fig. 10b)**. The effects of IACS-010759 on sensorimotor function were then assessed using the beam walk test[27]. Compared to vehicle-treated mice, mice treated with IACS-010759 took longer to cross the small round rod (**Extended Data Fig. 10c**), indicating a decrease in balance and fine motor function. IACS-010759 treatment did not affect crossing

time on wide or narrow rectangular rods, indicating no effect of treatment on motivation to perform the task (**Extended Data Fig. 10c**). Overall, these findings demonstrate that, similar to clinical findings, IACS-010759 induces signs of peripheral neuropathy at a clinically relevant exposure.

Next, we investigated the association between peripheral neuropathy and mitochondrial dysfunction in peripheral sensory neurons. Strikingly, IACS-010759 treatment dose-dependently inhibited OCR in dorsal root ganglia (DRG) that were collected 3-4 hours after the last dose (**Fig 5e**) and at 5 weeks after the last dose (**Fig 5f, Extended Data Fig. 10d**) of IACS-010759. The highest dose of IACS-010759 tested also reduced intraepidermal nerve fiber density (IENF) in the hind paw skin, a marker of peripheral neuropathy that is sensitive to mitochondrial dysfunction[28,29] (**Extended Data Fig. 10e**). Of note, expression of ATF3, a transcription factor that initiates the nerve regeneration pathway and is induced after traumatic nerve injury [30], did not increase upon IACS-010759 treatment, indicating that neuronal degeneration did not occur (**Extended Data Fig. 10f**). Finally, the effects of IACS-010759 on the sciatic nerve of mice was determined with electronic microscopy analysis at five weeks after completion of vehicle or 5 mg/kg IACS-010759 treatment. In line with what was observed in patients, IACS-010759 treatment resulted in myelin damage that was characterized by the decompaction of myelin and split sheets (**Extended Data Fig. 10g**).

In efforts to minimize treatment-induced peripheral neuropathy, we assessed the efficacy of co-administering IACS-010759 with the experimental HDAC6 inhibitor ACY-1215 (Ricolinostat), which has been shown to prevent and reverse chemotherapy-induced peripheral neuropathy[31]. C57/Bl6 mice were treated with 0.3 or 1 mg/kg of IACS-010759 with or without 30 mg/kg of ACY-1215, or with vehicle, for two weeks with a 5 on/2 off schedule, and mechanical allodynia was assessed 4 days after the last dosing. Co-administration of ACY-1215 significantly attenuated IACS-010759-induced mechanical allodynia (**Fig. 5g**), as well as prevented IACS-010759-induced spontaneous pain (**Extended Data Fig. 10h**), sensorimotor deficits (**Extended Data Fig. 10i)**, and damage to the myelin of the sciatic nerve (**Extended Data Fig. 10j**). However, co-administration with ACY-1215 did not prevent IACS-010759-induced reduction of OCR in the DRG (**Fig. 5e**). Together, these findings indicate that the neurotoxicity induced by IACS-010759 may occur through multiple mechanisms, and co-administration of ACY-1215 can be used to prevent some of the symptoms associated with treatment-induced peripheral neuropathy.

Discussion

Based on preclinical findings[15], two first-in-human Phase I clinical trials were initiated to assess the safety and efficacy of IACS-010759, a selective, small-molecule complex I inhibitor, in patients with AML or advanced solid tumors. Clinical trial findings revealed that the efficacious levels of plasma IACS-010759 determined from preclinical models could not be maintained with the implemented dosing regimens. Consequently, despite achieving modest on-target inhibition, IACS-010759 exposures were insufficient to reduce tumor burden in patients. Further, complex I inhibition resulted in the induction of resistance mechanisms in AML patients, as evidenced by increased levels of mitochondrial DNA in AML blasts upon prolonged IACS-010759 treatment. This finding suggested a compensatory increase in

mitochondria numbers in AML blasts that may be mediated by mitochondrial fission and/or by acquisition from bone marrow mesenchymal stem cells via tunneling nanotubes[25]. Taken together, our data indicated that patients with AML or solid tumors needed to achieve and maintain plasma exposures higher than those observed during the trials to clinically benefit from IACS-010759.

Mechanism-based toxicities related to elevated blood lactate and neurotoxicity prevented the further dose escalation and schedule intensification of IACS-010759. These toxicities have been also reported to limit the translation of complex I inhibitors such as ASP4132[14] and BAY 87-2243[5,32] for anti-cancer treatment. Here, the development of persistent and dose-dependent IACS-010759-induced peripheral neuropathy was the most significant contributor to the early termination of both trials. Together, these data underscore the necessity for evaluating treatment-induced neurotoxicity during the preclinical stage of developing drugs that target complex I.

Associations between dysfunctional metabolic pathways, particularly those that result in elevated plasma lactate, and dysfunction in the nervous system have previously been reported[28,33]. For instance, several studies support mitochondrial dysfunction in the primary sensory neurons of the DRG as a main contributor to chemotherapy-induced peripheral neuropathy[28,34,35,36,37,38]. We thus hypothesize that the peripheral neuropathy induced by IACS-010759 is primarily mediated by inhibited oxidative metabolism. Interestingly, elevated plasma lactate was a stronger predictor of peripheral neuropathy than plasma IACS-010759 concentrations in our patients (**Fig 2 d,e**). Elevated lactate is commonly observed upon OXPHOS inhibition[2,14,15,21,22], and indicates a compensatory increase in glycolysis to mitigate energetic stress[33,39]. In follow-up reverse translational studies, we demonstrated that co-administration of ACY-1215 (Ricolinostat), an experimental HDAC6 inhibitor, with IACS-010759 prevented treatment-induced behavioral changes indictive of peripheral neuropathy. Our data, in addition to other studies[31,35,38,40], thus support the exploration of combination approaches to prevent or mitigate the neurotoxic effects associated with mitotoxic agents.

Interestingly, the significant risk factors for developing IACS-010759-induced peripheral neuropathy among our patients have also been associated with neurotoxicity. This, potentially, suggests that some of our patients may have been sensitized to or harbored neural damage prior to enrollment. Specifically, among our AML patients, alloSCT was the strongest predictor for developing peripheral neuropathy. While rare, an association between alloSCT treatment and neurological complications, including peripheral neuropathy, has been observed in patients with hematologic malignacies[41-44]. This association is largely attributed to chronic graft versus host disease[41-43], but contributing factors also include immune system reconstitution[41], drug complications[41,44], prior neurological disease[41,44], the female sex[45], and total-body irridation[45]. Among patients in the Solid Tumor trial, the biggest predictors of developing peripheral neuropathy were prior chemotherapy and concomitant diagnosis of diabetes mellitus, two conditions widely associated with peripheral neuropathy[28,36]. Together, these associations suggest that future trials assessing the anti-tumoral capabilities of agents targeting complex I must account for previous therapies or pre-existing conditions that may have already caused neural damage. Regardless, our data emphasize

the necessity for a systematic evaluation of neurotoxicity for all novel investigational agents targeting complex I and similar mechanisms at the preclinical stage.

Overall, our findings raise concerns about the risks and feasibility of leveraging complex I inhibitors for anti-cancer therapy. Currently, at least 13 caomplex I inhibitors are being evaluated as anti-cancer agents in preclinical or clinical settings[5]. We urge researchers to critically assess for the neurotoxic effects of their mitotoxic agents prior to advancing the translation of their compound.

Methods

Patient selection and screening and eligibility

Patients eligible for the AML Trial were previously diagnosed with AML using the World Health Organization criteria as well as had either failed prior induction therapy (refractory AML), had a first relapse after prior therapy with a first remission duration of <12 months, or had relapsed to more than one prior AML therapy. Additional eligibility criteria included 1) age 18+ years; 2) Eastern Cooperative Oncology Group performance status ≤2; 3) completion of prior cytotoxic/non-cytotoxic agents and biological/immune-based therapies, including investigational agents, occurred at least 2 weeks or 5 half-lives interval –whichever was shorter– prior to start of trial; 4) adequate organ function (total bilirubin ≤2.0 x the upper limit of normal (ULN) or ≤3.0 x ULN if considered due to Gilbert's syndrome; ALT and AST ≤ 2.5 x ULN or ≤ 5.0 x ULN if due to leukemic involvement; serum creatinine ≤2.0 mg/dL x the ULN). Hydroxyurea was allowed for subjects with rapidly proliferative disease before the start of study therapy and for the first 2 cycles on therapy. Patients with blood lactate levels >2 mmol/L and/or serum pH <7.35 were excluded.

Patients eligible for the Solid Tumor Trial were males or non-pregnant women with a histologically confirmed advanced solid tumor or lymphoma that was metastatic or unresectable, and for which there was no available therapy likely to convey clinical benefit. Additional eligibility criteria included 1) age 18+ years, 2) having received at least one line of systemic therapy in the advanced/metastatic setting or who had a relapsed and/or refractory lymphoma with at least 2 prior lines of systemic therapy, and 3) were not candidates for high-dose therapy/autologous stem cell transplant.

Trial Design

The first IACS 010759 clinical trial ('AML Trial') was a first-in-human, open-label, phase I study that used a 3+3 dose escalation design. This design enabled the number of patients per cohort to be expanded beyond 3 patients at each dose level during the dose-escalation phase to better assess the pharmacokinetic (PK) and pharmacodynamic (PD) profiles of IACS-010759. The dose of 0.5 mg was selected as the starting dose in this first-in-human AML trial, which corresponded to no more than 1/10th of the level where no adverse effects were observed during pre-clinical toxicology studies. The initial dose of IACS-010759 for cohort 1 and 2 were 0.5 and 1.0 mg, respectively. For the first two cohorts, cycle 1

consisted of a single dose on Day 1 followed by a single dose on Day 8, and subsequent cycles consisted of daily doses. By contrast, cohorts 3 and 4 had induction doses of 2.0 mg and 2.5 mg, respectively, daily for Days 1-7, followed by a maintenance dose of 0.5 mg once per week and 1.0 mg thrice per week, respectively. For both cohorts, the maintenance dose was continued unless suspension or stopping criteria were met.

The second IACS-010759 clinical trial ('Solid Tumor Trial') was designed as an open-label phase 1 study. Each cycle comprised of 21 days and consisted of an initial induction phase in cycle 1 followed by a maintenance phase. During the induction phase, IACS-010759 was administered daily for the first 5 or 7 days depending on the dosing cohort being assessed. During the maintenance phase, IACS-010759 was administered with either once-a-week or twice-a-week doses. Dose escalation decisions were determined by the clinical trial Safety Monitoring Committee (SMC) based on toxicity, PK, PD, and antitumor activity. The doses and schedules of the induction and maintenance phases (Supplementary Table 1) were as follows: Cohort 1 received 2.0 mg QD of IACS-010759 for 7 days (induction), followed by 0.5 mg of IACS-010759 once-a-week (maintenance); Cohort 2: 2.5 mg QD of IACS-010759 for 7 days (induction), followed by 1.0 mg of IACS-010759 once-a-week (maintenance); Cohort 3: 3 mgs QD of IACS-010759 for 7 days (induction), followed by 3 mg of IACS-010759 once-a-week (maintenance); Cohort 4: 2.5 mg QD of IACS-010759 for 7 days (induction), followed by 2.5 mg of IACS-010759 twice-a-week maintenance; Cohort 5: 2.0 mgs QD of IACS-010759 for 7 days (induction), followed by 2.0 mg of IACS-010759 twice-a-week (maintenance); Cohort 6: 1.5 mg QD of IACS-010759 for 5 days (induction), followed by 1.5 mg of IACS-010759 twice per week (maintenance).

Both study designs and treatment plans are detailed in Supplementary Table 1.

Study Oversight

The Scientific Review Committee and Institutional Review Board at the University of Texas MD Anderson Cancer Center approved all protocols and amendments for the AML and Solid Tumor Trials, respectively. Both trials were conducted in accordance with the principles of the Declaration of Helsinki and the International Council for Harmonization Good Clinical Practice guidelines. For both trials, all patients provided written informed consent before enrollment. All authors contributed to data analysis and interpretation as well as to the preparation of the manuscript. A scientific writer employed by The University of Texas M.D. Anderson Cancer Center provided drafting and editorial assistance for the manuscript. Overall, all authors can confirm the accuracy and completeness of the study presented here.

Trial objectives and endpoints

The primary objective of the AML and Solid Tumor Trial was to determine the safety, tolerability, maximum tolerated dose (MTD) and recommended phase 2 dose (RP2D) of IACS-010759. For both trials, secondary objectives were to evaluate the PK and preliminary antitumor activity, including overall

response rate and duration of response. The exploratory objectives were to evaluate PD and any exploratory predictive biomarkers of IACS-010759 activity.

Safety and tolerability assessments

For both AML and Solid Tumor Trials, TEAEs and TRAEs were graded for severity according to the National Cancer Institute CTCAE v4.03. Given the potential for mechanistic toxicity of lactic acidosis during the AML trial, close monitoring of lactate, blood pH, and associated electrolytes was conducted in all patients. Any patient that presented with lactate levels >4 mmol/L, blood pH <7.30, and symptoms attributable to lactic acidosis (e.g. nausea, vomiting, generalized muscle weakness, tachycardia, hypotension, and rapid breathing) was hospitalized for closed monitoring for a minimum of 24 hours. However, patients who presented with lactate levels >4.0 mmol/L, blood pH <7.35, CO2 levels less than the lower limit of normal, an elevated anion gap, and/or symptoms of lactic acidosis were considered to have reached the dose limiting toxicity (DLT) upon confirmation of the results by arterial blood sampling. To reduce the variability of pH and lactate measurements, arterial blood gas and venous blood samples were immediately placed in an ice bath and all laboratory tests were performed within 30 minutes after samples were drawn. Upon completing the venous blood test, any sample showing lactic acidosis had to confirmed with an arterial blood gas, including the lactate results.

Determination of human plasma concentrations of IACS-010759

To measure IACS-10759 concentration in human plasma, aliquots of human plasma (50 µL) were first mixed with acetonitrile (200 µL) containing diclofenac as the internal standard (IS). This suspension was vortexed for 10 min and centrifuged at 4k rpm for 10 min, after which 100 µL of the extract was aliquoted and diluted with 100 µL of water prior to LC-MS/MS analysis. The UHPLC-MS/MS system consisted of a Shimadzu Nexara UHPLC system coupled with a Sciex 5500 triple quadrupole mass spectrometer operated at the positive mode (ESI+). The optimized source parameters were gas1, 35 psi; gas2, 50 psi; curtain gas, 35 psi; source temperature, 400°C; ion spray voltage, 5500 V. The separation of IACS-010759 was achieved on a Phenomenex Gemini C18 column (5µm, 110Å, 50x2.0mm) using a gradient mobile phase. Mobile phase A was acetonitrile and water (100/900, v/v) and mobile phase B was acetonitrile and methanol (500/500, v/v) containing 0.2% (v/v) formic acid. The LC gradient (%B) was 22% (0-0.3 min), 22-95% (0.3-1.3 min), 95% (1.3-2.3 min), 95-22% (2.3-2.31 min), and 22% B (2.31-3.0 min). Column temperature was set at 40 °C. Injection volume was 2 µL. IACS-10759 and IS were detected by a multiple reaction monitoring transition m/z 563.1 > 172.1 and m/z 295.9 > 151.2, respectively. Under these conditions, retention time was 1.52 min for IACS-010759 and 1.42 min for IS. The complete analytical run time was 5.0 min. This method was validated over the concentration range of 0.05 to 50.0 ng/mL of IACS-10759 in untreated human plasma.

AML blast collection, OCR analyses, mitochondrial DNA analyses

Fresh blood was obtained in BD Vacutainer™ Glass Blood Collection Tubes with Sodium Heparin ((Thermo Fisher Scientific : 026853B) and combined into a 50ml falcon tube to which equal volume of Easy Sep Buffer (StemCell Technologies: 20144) was added. This diluted blood was added to a Sepmate tube (StemCell Technologies, Catalog# 85450) containing 25 ml of Lymphoprep (StemCell Technologies: 07811). The tubes were centrifuged for 10 min at room temperature at 1200 rcf. The top layer was collected in a separate tube and, with 50 mL of Easy Sep Buffer added, centrifuged at 1800 rpm for 6 min at room temperature. The supernatant was discarded. 5-15 ml of Ammonium Chloride solution (StemCell Technologies: 07850) was added to the pellet, and the solution was gently rocked on a shaker for 10-15 minutes. Easy Sep Buffer was added after lysis and centrifuged. The pellet was resuspended in optimum volume of Easy Sep buffer and counted on a Cellometer Auto 1000 Bright Field Cell Counter (Nexcelcom Biosciences). PBMC samples were then depleted of CD3/CD19 positive population using the StemCell separation protocol and custom antibody cocktails (StemCell Technologies).

A single cell suspension of PBMCs at a concentration of $1x10^8$ cells/ml was prepared in EasySep Buffer in a round bottomed tube. To this, custom EasySep Human CD3/CD19 cocktail was added at a concentration of 100 µl/ml of cells. The suspension was vortexed for 10 seconds and incubated for 5 min at room temperature. Dextran Rapid Spheres (StemCell Technologies 50100) were then added at a concentration of 125 µl/ml of cells. The suspension was vortexed for 10 sec and incubated for 3 min at room temperature after which the final volume was made up to 2.5 ml and gently vortexed for 10 sec. The tube was then placed into the EasyEights magnet (StemCell Technologies : 18103) to separate for 10 min at room temperature. Using a 2 ml serological pipet, the cells were carefully collected into a new 5 ml round-bottom tube from the non-magnetic side without removing or moving the tube. The new tube was placed into the EasyEights magnet (StemCell Technologies: 18103) to separate for 10 min at room temperature. The cells (AML blasts) were carefully collected after the second round of suspension and an appropriate volume of PBS was added before counting on a Cellometer Auto 1000 Bright Field Cell Counter (Nexcelcom Biosciences). Blasts were immediately used for the Seahorse assay to measure changes in basal and maximal OCR, and the remaining were frozen in Bambanker cell freezing medium (Thermo Fisher Scientific : 50999554) before storing in liquid Nitrogen. Changes in mitochondrial DNA and genomic DNA were measured and analyzed with methods described in Rooney et al., 2015.[46]

Metabolomic Assays

Intracellular metabolites were extracted and then analyzed using UHPLC-MS/MS, as previously described[47,48]. Briefly, intracellular polar metabolites were extracted using a modified Bligh-Dyer procedure. All LC-MS analyses were performed on a Q Exactive Hybrid Quadrupole Orbitrap mass spectrometer (Thermo Scientific) coupled to a Vanquish Horizon UHPLC system (Thermo Scientific). Metabolite separation was performed using a SeQuant ZIC-HILIC 3.5µm, 100 Å, 150 × 2.1 mm column (Millipore Sigma) and a Kinetex C18,2.6µm, 100 Å, 150 × 2.1 mm column (Phenomenex). Pooled quality control samples were acquired every six samples to ensure optimal instrument performance and consistency. Raw files were processed using SIEVE 2.2.0 SP2 (Thermo Scientific), and the integrated

peaks were mined against an in-house database of accurate masses and retention times generated using the IROA 300, MS Metabolite Library of Standards (IROA Technologies), as well as accurate masses from the Human Metabolome database[49] and the KEGG database[50].

mRNA-seq library preparations and Sequencing

mRNA libraries were prepared and sequenced according to published methods[51]. Briefly, libraries were prepared with the Illumina TruSeq Stranded mRNA protocol starting with 1 µg total RNA. Purified mRNAs were then fragmented and converted to cDNA with reverse transcriptase. Resulting cDNAs were converted to double stranded cDNAs and subjected to end-repair, A-tailing, and adapter ligation. Constructed libraries were amplified using 8 cycles of PCR. The NuGEN Ovation RNA-Seq System v2 (Cat. # 7102–32) (NuGEN) was used to convert lTotal RNA (100 ng) to cDNA by following the manufacturer's protocol (NuGEN, San Carlos, CA). 2.8 nM of pooled libraries were then processed using a cBot (Illumina) for cluster generation before sequencing on an Illumina HiSeq 3000 (2 × 76 bp run).

RNA-sequencing analysis

Quality of the sequencing data was studied by use of the package fastqc (http://www.bioinformatics.babraham.ac.uk/projects/fastqc/). Sequences were then aligned to the human reference genome "GRCh38" (Ensembl Release 96 Databases, released on April 10, 2019) and quantified using Quasi-mapping mode by the package "salmon"[52], which calculated gene counts and abundances. Abundance data were then normalized by inter-library normalization, trimmed mean of M values (TMM)[53], which accounts for library size variation between samples of interest.. After alignment, only transcript IDs representing genes of standard chromosomes (1 to 22, X, Y, and MT) were kept, and transcript IDs that were not expressed across all samples (both count and abundance = 0) were removed. In addition, transcript IDs with both low counts and low standard deviations (SD), which may increase incidents of false positives, were removed. Further, we discounted all summarized gene counts other than those with raw counts > 2 and SD > 1. Overall, we obtained 106,209 transcript IDs that represented 19,323 unique genes.

All statistical analyses were performed using R version 3.5.1 (https://www.r-project.org/). For analyzing gene expression, we used a linear mixed effect model in which patients were used as random effects and treatment were used as the fixed effect. Due to multiple comparisons, the rate of type I errors was adjusted by using a false discovery rate (FDR) cutoff of < 0.05 (FDR)[54]. As such, 1,065 genes were identified to be significantly associated with treatments. An unsupervised hierarchical clustering analysis for which correlation was used as the distance metric and ward was used as the clustering method was employed to display the expression patterns of significant genes. To identify the functionality of genes of interest, we applied gene ontology (GO) enrichment analysis implemented in an R Package "GOsummaries"[55]. To investigate deregulated biological pathways, we downloaded pathways and gene

sets from MSigDB (http://www.gsea-msigdb.org/gsea/msigdb/index.jsp) and used an R package "seq2pathway"[56] to calculate pathway scores. A linear mixed effect model was then used to identify significant pathways.

Preparation of mouse models

To develop AML patient-derived xenograft (PDX) models, 55 adult female NSG mice (Jackson Laboratory, NOD.Cg-*Prkdc*^{scid} *Il2rg*^{tm1Wjl}*/SzJ*, Stock No: 005557) were injected intravenously with the PDX AML-04030094 model at 0.5 x 10^5 cells per mouse and then treated accordingly with clinically relevant doses of IAC-010759. Each mouse received exposure to Cesium-radiation at 250 cGY 24 hours prior to receiving the cell injection. Using an 1 ml syringe and 27 g needle, an intravenous injection of 200 µl (a concentration equal to 0.5 x 10^5 cells) was injected into the lateral tail vein.

To prepare mice for investigating treatment-induced peripheral neuropathy, male C57BL/6J mice (#000664, Jackson laboratory, Bar Harbor, ME) were housed on a 12 hour light/dark cycle (lights on 8:00 am) with free access to food and water.

All procedures were approved by the Institutional Animal Care and Use Committee (IACUC) of M.D. Anderson Cancer Center and are in accordance with National Institutes of Health (NIH) guidelines for the care and use of animals. All animals were maintained at the animal facility within The University of Texas MD Anderson Cancer Center. All analyses were performed by investigators blinded to treatment.

Effects of IACS-010759 on survival in AML PDX models

Investigation into whether IACS-010759 extends the survival of AML PDX models began when AML PDX mice exhibited a disease burden of 3% circulating in whole blood. Disease burden was determined by collecting approximately 125 µl of whole blood retro-orbitally from 10 unanesthetized mice into EDTA coated tubes and stored on wet ice for analysis. Forty-five mice were randomized into the following groups (n=9/group) and received assigned treatment: 1) vehicle (0.5% Methylcellulose), 2) 0.1 mg/kg IACS-010759, 3) 0.3 mg/kg IACS-010759, 4) 1 mg/kg IACS-010759, and 5) 5 mg/kg IACS-010759. Treatment 10 ml/kg was administered by oral gavage once per day for 5 days on and 2 days off treatment.

After 4 days of treatment, pharmacokinetics were assessed at 2 and 24 hours post-dose. Whole blood (~125 ul) was collected retro-orbitally from each unanesthetized mouse by placing a heparin lined capillary tube into the lateral canthus and slightly twisting the tube to cause blood to flow directly into EDTA-coated collection vials. Vials were then placed into a centrifuge for 5 minutes at 5000 g. Plasma was isolated using a Pipetman, transferred into a microfuge tube, then placed on dry ice. For long term storage, samples were stored under -80 ºC until analysis.

To measure the survival of treated mice, body weights were collected twice per week. Body condition was assessed when each mouse received its scheduled dose of compound. Disease progression in mice was indicated by loss of body weight, onset of hind-limb paralysis, lethargy, and hunched postures. A mouse was euthanized upon losing >20% of its original body weight or developing hind-limb paralysis. Immediately after euthanization, the spleen and plasma were collected and stored for future analyses.

Behavioral studies assessing treatment-induced peripheral neuropathy

To investigate the effects of treatment-induced peripheral neuropathy, mice were randomized into groups (n= 4-8/group) that received either IACS-010759 or vehicle (control). Depending on the experiment, mice received either 0.1, 0.3, 1.0, or 5.0 mg of IACS-010759 in 0.5% methyl cellulose or vehicle (control). To assess whether co-administration of the HDAC6 inhibitor ACY-1215 (Ricolinostat, Regenacy Pharmaceuticals) could mitigate treatment-induced neuropathy, mice were randomized into groups that received either IACS-010759 + ACY-1215, IACS-010759 alone, ACY-1215 alone, or vehicle (control) alone. When applicable, IACS-010759 was administered as previously described. When applicable, ACY-1215 (Ricolinostat) in 10% DMSO, 30% propylene glycol (#P4347, Sigma), and 60% poly(ethylene glycol)-300 (#81162, Sigma) was administered orally at a dose of 30 mg/kg 60 minutes before each dose of IACS-010759. All treatments for both experiments were administered by oral gavage once per day for five days on, two days off, followed by a second round of five days on.

Mechanical allodynia was quantified using von Frey calibrated filaments at Day 6 after the first dose and then for every 3 days for 24 days. The mechanical stimulus producing a 50% likelihood of withdrawal was determined using the “up-down” calculating method as previously described[57-59]

Spontaneous pain was measured using a conditioned place preference (CPP) paradigm with retigabine as the conditioned stimulus at two weeks after the last dose of treatment or vehicle **(Extended Data Fig. 9a**)[60]. At least one week before the CPP procedure, mice were housed in a reversed light/dark cycle (lights off at 8 am). The CPP apparatus consisted of 2 chambers (18 x 20 cm, one dark, one bright) connected by a 15 cm hallway (Stoelting, Wood Dale, IL). On Day 1, each mouse freely explored the apparatus for 15 min. Over the next four days, mice were conditioned to associate the light chamber with pain relief. In the morning, mice were injected i.p. with phosphate buffered saline (PBS), rested for 10 min, individually placed in the dark chamber for 20 min, and returned to their respective cages. Three hours later, mice were injected i.p. with 10 mg/kg of the analgesic drug retigabine (#R-100, Alomone laboratory, Jerusalem, Israel) and placed in the light chamber. On Day 6, drug-free mice explored the apparatus for 15 min. All tests were recorded by video. Change in the time spent in the bright (previously analgesic-paired) chamber at Day 6 as compared to that during Day 1 was quantified on video recordings. Increased time in the analgesic-paired chamber is interpreted as evidence of spontaneous pain.

Sensorimotor function was assessed by a beam-walking test after completion of the CPP test. On Day 1, mice were trained to cross a rectangular beam (85 cm in length with a flat surface of 1.2 cm in width) resting on two poles and elevated 40 cm above the table top. Over 3 consecutive trials, mice were placed at one end of the beam and were trained to cross to the escape platform on the other end. On Day 2, the time needed to cross the 1.2 cm beam was recorded in two trials. On the same day, mice were trained to cross a narrow rectangular beam (85 cm in length, 0.6 cm in width). On Day 3, time to cross the narrow rectangular beam was recorded in two trials. On the same day, mice were trained to cross a round beam (diameter 1.2 cm) until mice in the control group could cross the beam successfully in two consecutive trials. On the last day, the time to cross the round beam was recorded in two trials. All trials were taped, and the time to cross was analyzed by an investigator blinded to treatment and group. The beams and platform were cleaned with 70% ethanol before each new animal was tested.

Mitochondrial function of DRG neurons

Mice were sacrificed by CO2 overdose and DRG neurons were collected from each mouse 3-4 hours after the last dose or 5 weeks after the last dose of either IACS-010759 or vehicle. Mitochondrial bioenergetics of DRG neurons were measured with the XF24 Flux Analyzer (Agilent Technologies Inc, Santa Clara, CA) as previously described [3, 5]. DRG neurons were plated in XF24 microplates and cultured overnight in Ham's F-10 media (#10-070-CV, Corning, NY) with N2 supplement (#17502001, Thermo Fisher Scientific, Waltham, MA). On the day of the assay, media was changed to XF media supplemented with 5 mM glucose, 0.5 mM sodium pyruvate, and 1 mM glutamine (Agilent Technologies Inc) for OCR measurement. Oligomycin A (2 μM), carbonyl cyanide-p-trifluoromethoxyphenylhydrazone (FCCP; 4 μM), as well as rotenone and antimycin A (2 μM each) (Sigma-Aldrich) were used to determine mitochondrial respiratory properties. The results were normalized to the protein contents of each well.

Immunofluorescence

To quantify IENFs, the glabrous skin of the hind paws was collected at 12 days after the last dose and processed as described previously[61]. Frozen sections (25 μm) were incubated with rabbit anti-PGP9.5 (ab108986, 1:500) and goat anti-collagen IV antibodies (1340-01, 1:100, Southern Biotech, Birmingham, AL) followed by Alexa-594 donkey anti-rabbit and Alexa-488 donkey anti-goat secondary antibodies (Life Technologies, Carlsbad, CA). Images were captured with a Leica SPE confocal microscope (Leica Microsystems, Buffalo Grove, IL). IENF density was quantified as the total number of PGP9.5 stained nerve fibers that crossed the collagen-stained dermal-epidermal junction/length of epidermis (IENFs/mm). Eight mice from each group were measured, with five random pictures quantified from each mouse for individual IENF counts. Samples were then collected for ATF3 expression analysis 12 days after the last dose. Frozen sections (14 μm) of PFA-fixed, OCT embedded DRG were incubated overnight with anti-ATF3 antibody (Novus Biologicals #NBP-1-85816; 1:500) in PBS with 2% normal donkey serum and 0.1% saponin (Sigma, #S7900) followed by Alexa-fluo 594 donkey anti-rabbit antibody (A-21207)

and DAPI (Sigma, #D9542). ATF3 staining was visualized using a Leica SPE confocal microscope. DRG samples from mice that underwent spared nerve injury 2 weeks earlier served as positive controls.

Transmission electron microscopy (TEM) analysis of myelin integrity

For TEM analysis of myelin integrity, mice were euthanized with CO_2 and transcardially perfused with cold PBS. Each sciatic nerve was fixed in 2% glutaraldehyde (EM grade, #16220, Electron Microscopy Sciences) plus 2% PFA (EM grade, #15710, Electron Microscopy Sciences) in PBS for at least 24 hours. Fixed sampled were processed at the High Resolution Electron Microscopy Facility at M. D. Anderson Cancer Center. Briefly, samples were washed in 0.1 M sodium cacodylate buffer and treated with cacodylate buffered tannic acid, post-fixed with 1% buffered osmium and stained en bloc with 0.1% Millipore-filtered uranyl acetate. Samples were then dehydrated in increasing concentrations of ethanol and infiltrated, and embedded in LX-112 medium. Samples were then polymerized in 60 ºC over approximately 3 days. Ultrathin sections were cut using a Leica Ultracut microtome and then stained with uranyl acetate and lead citrate in a Leica EM Stainer. Stained samples were examined in a JEM 1010 transmission electron microscope (JEOL USA, Inc, Peabody, MA) using an accelerating voltage of 80 kV. Digital imaged were obtained using an AMT imaging system (Advanced Microscopy Techniques Corp., Danvers, MA).

Percent damaged myelin was quantified as the (number of axons with decompacted/loosened myelin / total number of myelinated axons) * 100. For myelin thickness, maximum myelin diameter was used to measure thickness. The g ratio was quantified as the ratio of axonal/axonal+myelin diameter.

Statistical analysis

Statistical analysis of differences between groups was performed in GraphPad 8.0 (San Diego, CA) using two-way analysis of variance (ANOVA), one-way ANOVA, paired or unpaired Student's t-test when appropriate. $P<0.05$ was considered statistically significant.

Declarations

Data availability

All data supporting this study are available from the corresponding author upon reasonable request.

Acknowledgements.

This research is in part supported by the MD Anderson Cancer Center Leukemia National Institutes of Health (NIH) SPORE P50 CA100632, the NIH R01 CA206210, CPRIT RP180309, the NIH Clinical Translational Science Award 1UL1TR003167, MD Anderson Cancer Center support grant (P30 CA016672), the Sheikh Ahmed Bin Zayed Al Nahyan Center for Pancreatic Cancer Grant, and the

Leukemia & Lymphoma Society through its Therapy Acceleration Program (TAP) and by the MD Anderson Moon Shots program. The CPRIT Core is supported by the CPRIT Core Facility Support Grants (#RP120348 & #RP170002).

Author contributions.

Clinical studies were designed and initiated by T. A. Y., N. D., F. M. B., C. K. M., C. P. V., T. P. H., P. J., J. R. Ma., and M. K. Collection and analysis of clinical data were conducted by T. A. Y., N. D., F. M. B., C. K. M., C. P. V., T. P. H., P. J., J. R. Ma., M. K., C. S., M. B. B., E. E. B., S. F., D. S. H., D. D. K., A. N. S. A. P-P., J. R., V. S., S. P., and A. T. Several patients were recruited by N. P., F. R., M. Y., E. J. J., M. O., K. S., P. B., N. B., and H. M. K. Pharmacokinetic analyses and related figures were generated by S. Gr., J. R. Ma., and Q. A. X. Pharmacodynamic analyses in AML blasts and related figures were generated by S. T., M. M., M. C., Q. Z., J. H., and A. L. Transcriptomic analyses, data analyses, and related figures were generated by C. P. V., C. A. B., and Z. J. Preclinical studies and related figures were generated by C. J. H., A. K., J. Z., J. P. G., M. E. D-F., and J. R. Mo. Manuscript was written by T. A. Y., N. D., F. M. B., C. P. V., T. H., P. J., J R. Ma., M. K., and S. Ga. All authors reviewed the manuscript prior to submission.

Competing interests.

Timothy A. Yap has received Grant/Research support (to the Institution) from AstraZeneca, Artios, Bayer, Beigene, BioNTech, BMS, Clovis, Constellation, Cyteir , Eli Lilly, EMD Serono, Forbius, F-Star, Artios, GlaxoSmithKline, Genentech, Haihe, ImmuneSensor, Ionis, Ipsen, Jounce, Karyopharm, KSQ, Kyowa, Merck, Novartis, Pfizer, Repare, Ribon Therapeutics, Regeneron, Rubius, Sanofi, Scholar Rock, Seattle Genetics, Tesaro and Vivace. He has served in a consulting or advisory role for AbbVie, AstraZeneca, Acrivon, Adagene, Almac, Aduro, Amphista, Artios, Athena, Atrin, Avoro, Axiom, Baptist Health Systems, Bayer, Beigene, Boxer, Bristol Myers Squibb, C4 Therapeutics, Calithera, Cancer Research UK, Clovis, Cybrexa, Diffusion, EMD Serono, F-Star, Genmab, Glenmark, GLG, Globe Life Sciences, GSK, Guidepoint, Idience, Ignyta, I-Mab, ImmuneSensor, Institut Gustave Roussy, Intellisphere, Jansen, Kyn, MEI pharma, Mereo, Merck, Natera, Nexys, Novocure, OHSU, OncoSec, Ono Pharma, Pegascy, PER, Pfizer, Piper-Sandler, Prolynx, Repare, resTORbio, Roche, Schrodinger, Theragnostics, Varian, Versant, Vibliome, Xinthera, Zai Labs and ZielBio. He is a stockholder in Seagen. Naval Daver has received research funding from Daiichi-Sankyo, Bristol-Myers Squibb, Pfizer, Gilead, Sevier, Genentech, Astellas, Daiichi-Sankyo, Abbvie, Hanmi, Trovagene, FATE therapeutics, Amgen, Novimmune, Glycomimetics, Trillium, and ImmunoGen and has served in a consulting or advisory role for Daiichi-Sankyo, Bristol-Myers Squibb, Arog, Pfizer, Novartis, Jazz, Celgene, AbbVie, Astellas, Genentech, Immunogen, Servier, Syndax, Trillium, Gilead, Amgen, Shattuck labs, and Agios. Marina Konopleva has received research funding from AbbVie, Genentech, F. Hoffman La-Roche, Eli Lilly, Cellectis, Calithera, Ablynx, Stemline Therapeutics, Agios, Ascentage, Astra Zeneca; Rafael Pharmaceutical; Sanofi, Forty-Seven and has served in a consulting or advisory role for AbbVie, Genentech, F. Hoffman La-Roche, Stemline Therapeutics, Amgen, Forty-Seven, Kisoji and; Janssen. IACS-010759 was developed by scientists at MD Anderson. If this drug becomes FDA approved and commercially available, MD Anderson will profit from its sale.

References

1 Baccelli, I. *et al.* Mubritinib Targets the Electron Transport Chain Complex I and Reveals the Landscape of OXPHOS Dependency in Acute Myeloid Leukemia. *Cancer Cell* **36**, 84-99 e88, doi:10.1016/j.ccell.2019.06.003 (2019).

2 Schockel, L. *et al.* Targeting mitochondrial complex I using BAY 87-2243 reduces melanoma tumor growth. *Cancer Metab* **3**, 11, doi:10.1186/s40170-015-0138-0 (2015).

3 Andrzejewski, S., Siegel, P. M. & St-Pierre, J. Metabolic Profiles Associated With Metformin Efficacy in Cancer. *Front Endocrinol (Lausanne)* **9**, 372, doi:10.3389/fendo.2018.00372 (2018).

4 Kuramoto, K. *et al.* Development of a potent and orally active activator of adenosine monophosphate-activated protein kinase (AMPK), ASP4132, as a clinical candidate for the treatment of human cancer. *Bioorg Med Chem* **28**, 115307, doi:10.1016/j.bmc.2020.115307 (2020).

5 Xu, Y., Xue, D., Bankhead, A., 3rd & Neamati, N. Why All the Fuss about Oxidative Phosphorylation (OXPHOS)? *J Med Chem* **63**, 14276-14307, doi:10.1021/acs.jmedchem.0c01013 (2020).

6 Rha, S. Y. *et al.* Phase I study of IM156, a novel potent biguanide oxidative phosphorylation (OXPHOS) inhibitor, in patients with advanced solid tumors. *Journal of Clinical Oncology* **38**, 3590-3590, doi:10.1200/JCO.2020.38.15_suppl.3590 (2020).

7 Sullivan, L. B. *et al.* Supporting Aspartate Biosynthesis Is an Essential Function of Respiration in Proliferating Cells. *Cell* **162**, 552-563, doi:10.1016/j.cell.2015.07.017 (2015).

8 Kuntz, E. M. *et al.* Targeting mitochondrial oxidative phosphorylation eradicates therapy-resistant chronic myeloid leukemia stem cells. *Nat Med* **23**, 1234-1240, doi:10.1038/nm.4399 (2017).

9 Stuani, L. *et al.* Mitochondrial metabolism supports resistance to IDH mutant inhibitors in acute myeloid leukemia. *J Exp Med* **218**, doi:10.1084/jem.20200924 (2021).

10 Dykens, J. A. *et al.* Biguanide-induced mitochondrial dysfunction yields increased lactate production and cytotoxicity of aerobically-poised HepG2 cells and human hepatocytes in vitro. *Toxicol Appl Pharmacol* **233**, 203-210, doi:10.1016/j.taap.2008.08.013 (2008).

11 Bridges, H. R., Jones, A. J., Pollak, M. N. & Hirst, J. Effects of metformin and other biguanides on oxidative phosphorylation in mitochondria. *Biochem J* **462**, 475-487, doi:10.1042/BJ20140620 (2014).

12 Sanchez, M., Gastaldi, L., Remedi, M., Caceres, A. & Landa, C. Rotenone-induced toxicity is mediated by Rho-GTPases in hippocampal neurons. *Toxicol Sci* **104**, 352-361, doi:10.1093/toxsci/kfn092 (2008).

13 Trotta, A. P. *et al.* Disruption of mitochondrial electron transport chain function potentiates the pro-apoptotic effects of MAPK inhibition. *J Biol Chem* **292**, 11727-11739, doi:10.1074/jbc.M117.786442 (2017).

14 Janku, F. *et al.* First-in-human evaluation of the novel mitochondrial complex I inhibitor ASP4132 for treatment of cancer. *Invest New Drugs*, doi:10.1007/s10637-021-01112-7 (2021).

15 Molina, J. R. *et al.* An inhibitor of oxidative phosphorylation exploits cancer vulnerability. *Nat Med* **24**, 1036-1046, doi:10.1038/s41591-018-0052-4 (2018).

16 Chung, I. *et al.* Cork-in-bottle mechanism of inhibitor binding to mammalian complex I. *Sci Adv* **7**, doi:10.1126/sciadv.abg4000 (2021).

17 Samudio, I. *et al.* Pharmacologic inhibition of fatty acid oxidation sensitizes human leukemia cells to apoptosis induction. *J Clin Invest* **120**, 142-156, doi:10.1172/JCI38942 (2010).

18 Lagadinou, E. D. *et al.* BCL-2 inhibition targets oxidative phosphorylation and selectively eradicates quiescent human leukemia stem cells. *Cell Stem Cell* **12**, 329-341, doi:10.1016/j.stem.2012.12.013 (2013).

19 Boultwood, J. *et al.* Amplification of mitochondrial DNA in acute myeloid leukaemia. *Br J Haematol* **95**, 426-431, doi:10.1046/j.1365-2141.1996.d01-1922.x (1996).

20 Lissanu Deribe, Y. *et al.* Mutations in the SWI/SNF complex induce a targetable dependence on oxidative phosphorylation in lung cancer. *Nat Med* **24**, 1047-1057, doi:10.1038/s41591-018-0019-5 (2018).

21 Piel, S., Ehinger, J. K., Elmer, E. & Hansson, M. J. Metformin induces lactate production in peripheral blood mononuclear cells and platelets through specific mitochondrial complex I inhibition. *Acta Physiol (Oxf)* **213**, 171-180, doi:10.1111/apha.12311 (2015).

22 Bando, K. *et al.* Comparison of potential risks of lactic acidosis induction by biguanides in rats. *Regul Toxicol Pharmacol* **58**, 155-160, doi:10.1016/j.yrtph.2010.05.005 (2010).

23 Dohner, H. *et al.* Diagnosis and management of AML in adults: 2017 ELN recommendations from an international expert panel. *Blood* **129**, 424-447, doi:10.1182/blood-2016-08-733196 (2017).

24 Nishino, M., Jagannathan, J. P., Ramaiya, N. H. & Van den Abbeele, A. D. Revised RECIST guideline version 1.1: what oncologists want to know and what radiologists need to know. *American Journal of Roentgenology* **195**, 281-289 (2010).

25 Saito, K. *et al.* Exogenous mitochondrial transfer and endogenous mitochondrial fission facilitate AML resistance to OxPhos inhibition. *Blood Adv*, doi:10.1182/bloodadvances.2020003661 (2021).

26 Deuis, J. R., Dvorakova, L. S. & Vetter, I. Methods Used to Evaluate Pain Behaviors in Rodents. *Front Mol Neurosci* **10**, 284, doi:10.3389/fnmol.2017.00284 (2017).

27 Curzon, P., Zhang, M., Radek, R. J. & Fox, G. B. in *Methods of Behavior Analysis in Neuroscience Frontiers in Neuroscience* (eds nd & J. J. Buccafusco) (2009).

28 Bennett, G. J., Doyle, T. & Salvemini, D. Mitotoxicity in distal symmetrical sensory peripheral neuropathies. *Nat Rev Neurol* **10**, 326-336, doi:10.1038/nrneurol.2014.77 (2014).

29 Ma, J., Kavelaars, A., Dougherty, P. M. & Heijnen, C. J. Beyond symptomatic relief for chemotherapy-induced peripheral neuropathy: Targeting the source. *Cancer* **124**, 2289-2298, doi:10.1002/cncr.31248 (2018).

30 Kiryu-Seo, S. & Kiyama, H. Mitochondrial behavior during axon regeneration/degeneration in vivo. *Neurosci Res* **139**, 42-47, doi:10.1016/j.neures.2018.08.014 (2019).

31 Krukowski, K. *et al.* HDAC6 inhibition effectively reverses chemotherapy-induced peripheral neuropathy. *Pain* **158**, 1126-1137, doi:10.1097/j.pain.0000000000000893 (2017).

32 Kirkpatrick, D. L. & Powis, G. Clinically Evaluated Cancer Drugs Inhibiting Redox Signaling. *Antioxid Redox Signal* **26**, 262-273, doi:10.1089/ars.2016.6633 (2017).

33 Jha, M. K., Lee, I. K. & Suk, K. Metabolic reprogramming by the pyruvate dehydrogenase kinase-lactic acid axis: Linking metabolism and diverse neuropathophysiologies. *Neurosci Biobehav Rev* **68**, 1-19, doi:10.1016/j.neubiorev.2016.05.006 (2016).

34 Flatters, S. J. L. & Bennett, G. J. Studies of peripheral sensory nerves in paclitaxel-induced painful peripheral neuropathy: evidence for mitochondrial dysfunction. *Pain* **122**, 245-257, doi:10.1016/j.pain.2006.01.037 (2006).

35 Maj, M. A., Ma, J., Krukowski, K. N., Kavelaars, A. & Heijnen, C. J. Inhibition of Mitochondrial p53 Accumulation by PFT-mu Prevents Cisplatin-Induced Peripheral Neuropathy. *Front Mol Neurosci* **10**, 108, doi:10.3389/fnmol.2017.00108 (2017).

36 Xiao, W. H. & Bennett, G. J. Effects of mitochondrial poisons on the neuropathic pain produced by the chemotherapeutic agents, paclitaxel and oxaliplatin. *Pain* **153**, 704-709, doi:10.1016/j.pain.2011.12.011 (2012).

37 Zheng, H., Xiao, W. H. & Bennett, G. J. Mitotoxicity and bortezomib-induced chronic painful peripheral neuropathy. *Exp Neurol* **238**, 225-234, doi:10.1016/j.expneurol.2012.08.023 (2012).

38 Krukowski, K., Nijboer, C. H., Huo, X., Kavelaars, A. & Heijnen, C. J. Prevention of chemotherapy-induced peripheral neuropathy by the small-molecule inhibitor pifithrin-mu. *Pain* **156**, 2184-2192, doi:10.1097/j.pain.0000000000000290 (2015).

39 Gillies, R. J., Robey, I. & Gatenby, R. A. Causes and consequences of increased glucose metabolism of cancers. *J Nucl Med* **49 Suppl 2**, 24S-42S, doi:10.2967/jnumed.107.047258 (2008).

40 Durante, M. *et al.* Adenosine A3 agonists reverse neuropathic pain via T cell-mediated production of IL-10. *J Clin Invest* **131**, doi:10.1172/JCI139299 (2021).

41 Ruzhansky, K. M. & Brannagan, T. H., 3rd. Neuromuscular complications of hematopoietic stem cell transplantation. *Muscle Nerve* **52**, 480-487, doi:10.1002/mus.24724 (2015).

42 Sakellari, I. *et al.* Neurological adverse events post allogeneic hematopoietic cell transplantation: major determinants of morbidity and mortality. *J Neurol* **266**, 1960-1972, doi:10.1007/s00415-019-09372-3 (2019).

43 Koeppen, S., Thirugnanasambanthan, A. & Koldehoff, M. Neuromuscular complications after hematopoietic stem cell transplantation. *Support Care Cancer* **22**, 2337-2341, doi:10.1007/s00520-014-2225-0 (2014).

44 Dowling, M. R. *et al.* Neurologic complications after allogeneic hematopoietic stem cell transplantation: risk factors and impact. *Bone Marrow Transplant* **53**, 199-206, doi:10.1038/bmt.2017.239 (2018).

45 Siegal, D. *et al.* Central nervous system complications after allogeneic hematopoietic stem cell transplantation: incidence, manifestations, and clinical significance. *Biol Blood Marrow Transplant* **13**, 1369-1379, doi:10.1016/j.bbmt.2007.07.013 (2007).

46 Rooney, J. P. *et al.* PCR based determination of mitochondrial DNA copy number in multiple species. *Methods Mol Biol* **1241**, 23-38, doi:10.1007/978-1-4939-1875-1_3 (2015).

47 Lodi, A. *et al.* Combinatorial treatment with natural compounds in prostate cancer inhibits prostate tumor growth and leads to key modulations of cancer cell metabolism. *NPJ Precis Oncol* **1**, doi:10.1038/s41698-017-0024-z (2017).

48 Stanford, S. M. *et al.* The low molecular weight protein tyrosine phosphatase promotes adipogenesis and subcutaneous adipocyte hypertrophy. *J Cell Physiol* **236**, 6630-6642, doi:10.1002/jcp.30307 (2021).

49 Wishart, D. S. *et al.* HMDB: the Human Metabolome Database. *Nucleic Acids Res* **35**, D521-526, doi:10.1093/nar/gkl923 (2007).

50 Okuda, S. *et al.* KEGG Atlas mapping for global analysis of metabolic pathways. *Nucleic Acids Res* **36**, W423-426, doi:10.1093/nar/gkn282 (2008).

51 Chao, H. P. *et al.* Systematic evaluation of RNA-Seq preparation protocol performance. *BMC Genomics* **20**, 571, doi:10.1186/s12864-019-5953-1 (2019).

52 Patro, R., Duggal, G., Love, M. I., Irizarry, R. A. & Kingsford, C. Salmon provides fast and bias-aware quantification of transcript expression. *Nat Methods* **14**, 417-419, doi:10.1038/nmeth.4197 (2017).

53 Robinson, M. D. & Oshlack, A. A scaling normalization method for differential expression analysis of RNA-seq data. *Genome Biol* **11**, R25, doi:10.1186/gb-2010-11-3-r25 (2010).

54 Benjamini, Y. & Hochberg, Y. Controlling the False Discovery Rate: A Practical and Powerful Approach to Multiple Testing. *Journal of the Royal Statistical Society: Series B (Methodological)* **57**, 289-300, doi:https://doi.org/10.1111/j.2517-6161.1995.tb02031.x (1995).

55 Kolde, R. & Vilo, J. GOsummaries: an R Package for Visual Functional Annotation of Experimental Data. *F1000Res* **4**, 574, doi:10.12688/f1000research.6925.1 (2015).

56 Wang, B., Cunningham, J. M. & Yang, X. H. Seq2pathway: an R/Bioconductor package for pathway analysis of next-generation sequencing data. *Bioinformatics* **31**, 3043-3045, doi:10.1093/bioinformatics/btv289 (2015).

57 Chaplan, S. R., Bach, F. W., Pogrel, J. W., Chung, J. M. & Yaksh, T. L. Quantitative assessment of tactile allodynia in the rat paw. *J Neurosci Methods* **53**, 55-63, doi:10.1016/0165-0270(94)90144-9 (1994).

58 Singhmar, P. *et al.* The fibroblast-derived protein PI16 controls neuropathic pain. *Proc Natl Acad Sci U S A* **117**, 5463-5471, doi:10.1073/pnas.1913444117 (2020).

59 Ma, J. *et al.* Cell-specific role of histone deacetylase 6 in chemotherapy-induced mechanical allodynia and loss of intraepidermal nerve fibers. *Pain* **160**, 2877-2890, doi:10.1097/j.pain.0000000000001667 (2019).

60 Laumet, G. *et al.* Interleukin-10 resolves pain hypersensitivity induced by cisplatin by reversing sensory neuron hyperexcitability. *Pain* **161**, 2344-2352, doi:10.1097/j.pain.0000000000001921 (2020).

61 Mao-Ying, Q. L. *et al.* The anti-diabetic drug metformin protects against chemotherapy-induced peripheral neuropathy in a mouse model. *PLoS One* **9**, e100701, doi:10.1371/journal.pone.0100701 (2014).

Table

Table 1. Clinical characteristics and the onset of neurotoxicity in the 40 patients who received IACS-010759 treatment. Abbreviations: N, number of patients; NP, neuropathy; %, percentage.

		Solid Tumors				AML			
Factor	Category	NP	Non-NP	Chi-square statistic	p-value	NP	Non-NP	Chi-square statistic	p-value
Risk Factors for NP (N, %)	Prior chemotherapy: platinum or taxanes	11 (100)	4 (33)	**7.988**	**0.005**	1 (17)	-	-	-
	Prior stem cell transplantation	-	-	-	-	5 (83)	1 (9)	**9.370**	**0.002**
	Diabetes mellitus	5 (45)	1 (8)	**4.102**	**0.043**	1 (17)	5 (45)	1.410	0.235
	Hypothyroidism	1 (9)	1 (8)	0.004	0.949	-	2 (18)	-	-
	Prior checkpoint inhibitor	4 (36)	2 (17)	1.154	0.283	1 (17)	1 (9)	0.215	0.643
Lactate (mmol/L)	Average lactate level before OXPHOS	1.2	1.4	-	-	1.3	1.3	-	-
	Average highest lactate level during OXPHOS	4.5	2.6	-	-	3.9	3.0	-	-
Glycemia (mg/dL)	Level before OXPHOS	144	92			114	119		
	Level>140 (n)	5	0	4.102	0.428	1	3	0.243	0.622
	Level<140 (n)	6	12			5	8		
OXPHOS dosing (N, %)	0.5 mg/day	-	-			-	5 (41)		
	1.0 mg/day	-	2 (17)			2 (33)	1 (9)		
	1.5 mg/day	-	2 (17)			-	-	0.701	0.402
	2.0 mg/day	4 (36)	7 (58)	1.983	0.159	1 (17)	2 (17)		
	2.5 mg/day	4 (36)	1 (8)			3 (50)	3 (25)		
	3.0 mg/day	3 (27)	-			-	-		
Neuropathy (N, %)	Overall	11 (48)	12 (52)			6 (35)	11 (65)		
	Grade 1	7 (31)				4 (23)			
	Grade 2	3 (13)				-			
	Grade 3	1 (4)				2 (12)			

Extended Data Figure Legends

Extended Data Figure 1. Flow diagram depicting the two Phase I trials. Flow diagram depicts the disposition of patients through the trials in patients with AML (left) and in patients with advanced solid tumor or lymphoma (right). QD: once daily.

Extended Data Figure 2. Effect of IACS-010759 on venous lactate and blood pH. (a-d) Relationship between venous lactate and IACS-010759 concentrations in AML (a) cohort 1, (b) cohort 2, (c) cohort 3,

and (d) cohort 4. Dotted line indicates 8 nM of plasma IACS-010759. **(e-h)** Relationship between blood pH and plasma IACS-010759 concentrations in AML (e) cohort 1, (f) cohort 2, (g) cohort 3, and (h) cohort 4. Dotted line indicates 8 nM of plasma IACS-010759. **(i-m)** Relationship between venous lactate and IACS-010759 concentrations in Solid Tumor (i) cohort 1, (j) cohort 2, (k) cohort 3, (l) cohort 4, and (m) cohort 5. Dotted line indicates 8 nM of plasma IACS-010759. **(n-r)** Relationship between blood pH and plasma IACS-010759 concentrations in Solid Tumor (n) cohort 1, (o) cohort 2, (p) cohort 3, (q) cohort 4, and (r) cohort 5. Dotted line indicates 8 nM of plasma IACS-010759.

Extended Data Figure 3. Treatment-induced peripheral neuropathy. (a-b) (a) Ultrastructural examination and (b) electronic microscopy analysis of a biopsy collected from the left superficial peroneal upper leg nerve root of a Cohort 4 patient from the Solid Tumor trial. The patient developed Grade 3-4 peripheral neuropathy while on a treatment regimen of 2.5 mg of IACS-010759 daily during the induction phase (Day 1-7), and 2.5 mg bi-weekly during the maintenance phase. Images indicate severe vacuolar changes in myelin sheath with axonal degenerative changes and atrophy.

Extended Data Figure 4. Plasma IACS-010759 concentrations in individual patients. (a-b) Plasma IACS-010759 concentrations AML patients in (a) cohorts 1 (red) and 2 (blue), which received once daily (QD) dosing, and in (b) cohorts 3-4, which each received an induction and maintenance phase. **(e-f)** Plasma IACS-010759 concentrations in Solid Tumor (c) cohorts 1 and 5, (d) cohorts 2 and 4, (e) cohort 3, and (f) cohort 6. All cohorts received induction and maintenance phases.

Extended Data Figure 5. Correlations between plasma IACS-010759 concentration and baseline oxygen consumption rate (OCR) from AML blasts. Baseline OCR has been normalized to cell number. Each symbol represents the mean +/- 95% confidence interval derived from 2-6 technical replicates. Closed circles are predose and open circles indicate post dose values. Blue indicates pre-dose (C1D1). Red indicates after one week of QD dosing (C1D7 - Cohorts 3, 4; C1D14 - Cohorts 1, 2). Black closed circles are other timepoints collected during cycle 1. Correlations analyzed by a Pearson's correlation coefficient test; $p < 0.05$.

Extended Data Figure 6. Correlations between plasma IACS-010759 concentration and maximal oxygen consumption rate (OCR) from AML blasts. Maximal OCR has been normalized to cell number. Each symbol represents the mean +/- 95% confidence interval derived from 2-6 technical replicates. Closed circles are predose and open circles are post dose values. Blue indicates pre-dose (C1D1). Red indicates after one week of QD dosing (C1D7 - Cohorts 3, 4; C1D14 - Cohorts 1, 2). Black closed circles are other timepoints collected during cycle 1. Correlations analyzed by a Pearson's correlation coefficient test; $p < 0.05$.

Extended Data Figure 7. Evidence of target inhibition in AML blasts. (a-e) Effect of IACS-010759 on levels of (a) NAD+, (b) nicotinamide, (c) tryptophan, (d) glutamine, or (e) alanine in AML blasts from Patients 16, 17, and 19 from AML Cohort 4. Y-axis shows metabolite levels relative to pre-dose levels. Differences from pre-trial levels analyzed by linear regression; *$p < 0.05$, **$p < 0.01$, ***$p < 0.001$. **(g-f)** Effect of IACS-010759 exposure on NMP, NDP, and NTP levels in AML blasts from (g) Patient 16 and (f) Patient 19 from

AML cohort 4. Y-axis shows nucleotide levels respective to pre-dose levels. Differences from pre-trial levels analyzed by linear regression; *p < 0.05; **p < 0.01, ***p < 0.001.

Extended Data Figure 8. Drug-induced effects on gene expression in AML blasts. **(a)** Gene Ontology enrichment analysis on RNA-sequencing (RNA-seq) results from AML blasts collected from Patients 16, 17, and 19 of AML Cohort 4 at several pre- and post-dose timepoints across Cycle 1. **(b)** Pathway analysis ranking deregulated biological pathways upon IACS-010759 treatment from patients described in (a).

Extended Data Figure 9. Determining the target concentration of IACS-010759. Effect of escalating doses of IACS-010759 or vehicle on plasma lactate in B6 mice. Significant differences from lactate levels in vehicle-treated mice were analyzed by unpaired Student's T-test; n.s. = non-significant. Data shown as mean ± SE.

Extended Data Figure 10. Reverse translational studies. (a) Schematic of the Conditioned Place Preference Test used to assess spontaneous pain. On Day 1, the mouse roamed between light and dark chambers. On Days 2-5, the mouse learned to associate pain relief (retigabine treatment) with the light chamber, and lack of pain relief (PBS treatment) with the dark chamber. On Day 6, the mouse was given the experimental treatment and allowed to roam freely, with relatively more time spent in the light chamber, indicating pain-relief seeking behavior**. (b)** Spontaneous pain assessed with a CPP (a) test at 2 weeks after the last dose of IACS-010759 (n=6) or vehicle (n=6). Mice were treated with two rounds of daily IACS-010759 or vehicle doses for 5 days on (grey) and 2 days off. Data reflect the change in time spent in the light (retigabine-paired) chamber. Data are analyzed by Student's T-test; ***p<0.001. Data shown as mean ± SE. **(c)** Sensorimotor function of mice in (b) was assessed with a beam walk test with a wide rectangular, narrow rectangular, or round rod. Data represent time to cross the beam. Data were analyzed with a two-way repeated measures ANOVA with Sidak's multiple comparison test; *p=0.01. Data shown as mean ± SE. **(d)** Oxygen consumption rate (OCR) in the dorsal root ganglion (DRG) neurons from mice in (b) measured under basal conditions (Basal) and after addition of oligomycin (ATP), FCCP (Max), or Actinomycin + Rotenone (H+ leak). Measurements taken using Seahorse technology at 5 weeks after the last dose of IACS-010759 or vehicle. Data shown as mean ± SE. **(e)** Density of intraepidermal nerve fibers (IENF) from mice in (b) was assessed at 12 days after the last dose by quantifying the number of PGP9.5 and nerve fibers crossing into the hind paw epidermis per length (mm) of the basement membrane. Data analyzed by one-way ANOVA followed by Dunnett's multiple comparison test; *p<0.05. Data shown as mean ± SE. **(f)** Immunohistochemistry analysis of ATF3 expression (pink) in the dorsal root ganglion of mice treated with vehicle (negative control), 1 mg/kg of IACS-010759, or 5 mg/kg of IACS-010759. A spare nerve injury (SNI) with clear ATF3 staining served as the position control. Scale bar = 167.2 μm. **(g)** Representative transmission electron microscopy cross sections of the sciatic nerve from mice in (b) at 5 weeks after the last dose of vehicle (top; n=205 axons/4 mice) or IACS-010759 (bottom; n=131 axons/4 mice). Arrows indicate areas of split myelin, arrowheads indicate vacuoles in myelin sheet. (right) Comparison of effects of IACS-010759 on myelin. Mild: occasional split sheet; moderate: many split sheets; severe: many split sheets and vacuoles. Difference vs controls analyzed by Fisher's exact test; ***p<0.001, **p<0.01, *p< 0.05. **(h)** Spontaneous pain assessed with a CPP test (a) at 2 weeks

after the last dose of IACS-010759 or vehicle +/- ACY-1215. Mice were given two rounds of daily treatment for 5 days on and 2 days off. ACY-1215 or vehicle was administered 1 hour before IACS-010759 or vehicle. Differences were analyzed by a two-way ANOVA, ***p<0.001. Data show mean ± SE; Dots indicate measurements from individual mice. **(i)** Sensorimotor function of mice in (h) was assessed with a beam walk test using a round rod at 2 weeks after the last dose of IACS-010759 or vehicle +/- ACY-1215. Data represent time to cross the beam. Differences analyzed by repeated-measures two-way ANOVA with Dunnett's Multiple comparison test; ****P<0.0001, ***P<0.001. Data show mean ± SE; Dots indicate measurements from individual mice. **(j)** (left) Representative transmission electron microscopy cross sections of the sciatic nerve from mice in (h) at 5 weeks after the last dose of vehicle (top; n=184 axons/4 mice), IACS-010759 (center; n=158 axons/4 mice), or IACS-010759 + ACY-1215 (bottom; n=201 axons/4 mice). Arrows indicate areas of split myelin, arrowheads indicate vacuoles in myelin sheet. (Right) Comparison of effects induced by vehicle, 0.3 mg/kg IACS-010759 (n=233 axons/4 mice), 1 mg/kg IACS 010759, 1 mg/kg IACS-010759 + ACY1215, or ACY-1215 (n=255 axons/4 mice) on myelin. Mild: occasional split sheet; moderate: many split sheets; severe: many split sheets and vacuoles. Analysis by Fisher's exact test; **p < 0.01 vs control; $^{\#\#}$p < 0.01 vs 1 mg/kg IACS-010759.

Figures

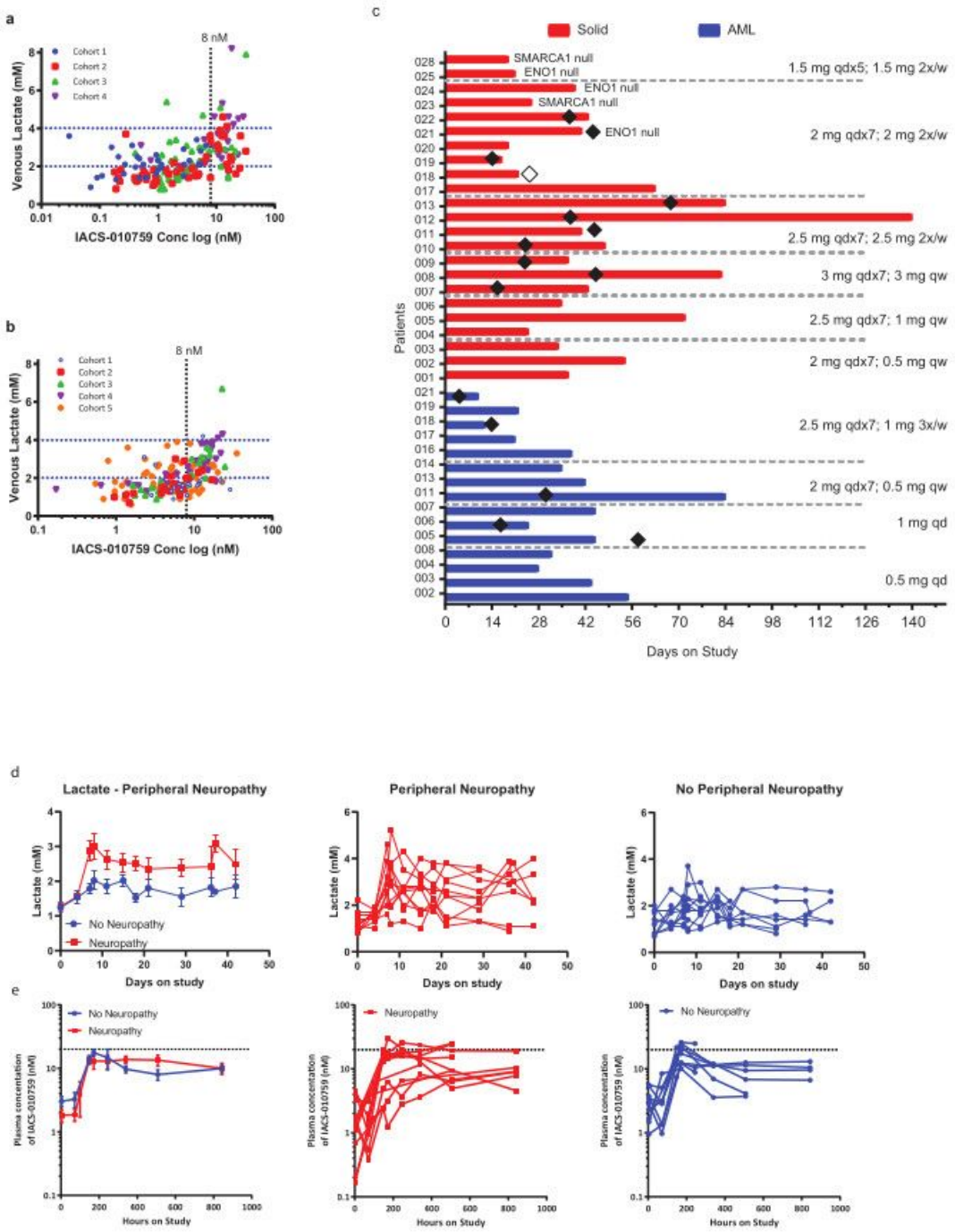

Figure 1

Figure 1

Drug-related toxicity. **(a-b)** Change in venous lactate levels across plasma IACS-010759 concentrations in (a) AML cohorts and (b) Solid Tumor cohorts. Each dot represents the mean value of all samples collected from the cohort at the same time point. **(c)** Study timelines of patients from the Solid Tumor (red) or AML (blue) trials. Onset of peripheral neuropathy is indicated by a diamond. Myagia and muscle weakness indicated by open diamond. Patients with SMARCA1-null or ENO1-null tumors are noted.

Dosing regimen indicated on the right. **(d)** (left) Comparison of plasma lactate levels in Solid Tumor patients who developed (red) or did not develop (blue) peripheral neuropathy. Differences compared to pre-trial plasma levels were calculated with a linear regression; *p < 0.05. Data show mean ± SE. Individual comparisons of plasma lactate levels in Solid Tumor patients who (center) developed or (right) did not develop peripheral neuropathy. **(e)** (left) Comparison of plasma IACS-010759 concentrations in Solid Tumor patients who developed (red) or did not develop (blue) peripheral neuropathy. Differences compared to pre-trial plasma levels were calculated with a linear regression; *p < 0.05. Data show mean ± SE. Individual comparisons of plasma IACS-010759 levels in Solid Tumor patients who (center) developed or (right) did not develop peripheral neuropathy.

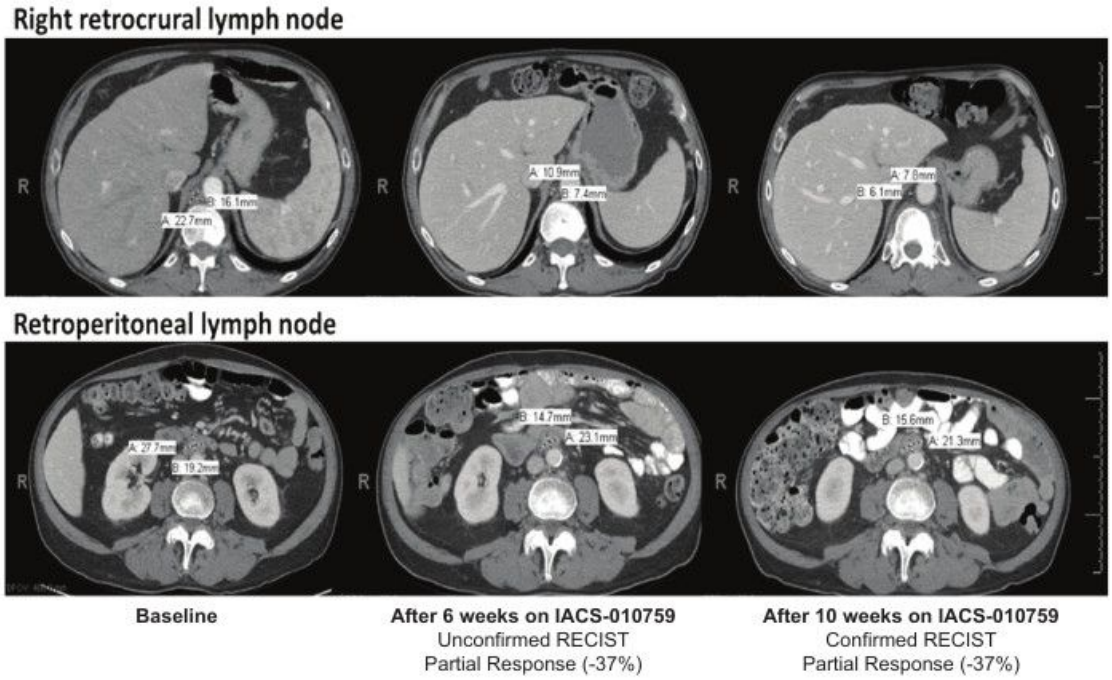

Figure 2

Figure 2

Radiological and clinical benefit in patient with advanced castration-resistant prostate cancer (CRPC). A patient with heavily pretreated CRPC achieved a confirmed RECIST v1.1 partial response with resolution of cancer-related pain. Restaging computed tomography (CT) scans done after two 3-week-long cycles of IACS-010759 showed reduction in sizes of a right retrocrural lymph node (top panel: 1.6 to 0.7 cm) and a retroperitoneal lymph node (bottom panel: 1.9 to 1.5 cm), with stabilization of bony metastases. These

radiological findings were then confirmed as a RECIST v1.1 partial response on his subsequent CT scan a month later. Unfortunately, this patient developed grade 3 IACS-010759-related peripheral neuropathy, leading to a prolonged drug hold and subsequent disease progression that resulted in trial discontinuation after 4 months on trial. This patient was heavily pretreated, having previously received radiation as well as systemic therapies comprising lupron, casodex, sipuleucel-T, abiraterone, ipilimumab and nivolumab, cyclophosphamide, as well as vincristine and dexamethasone.

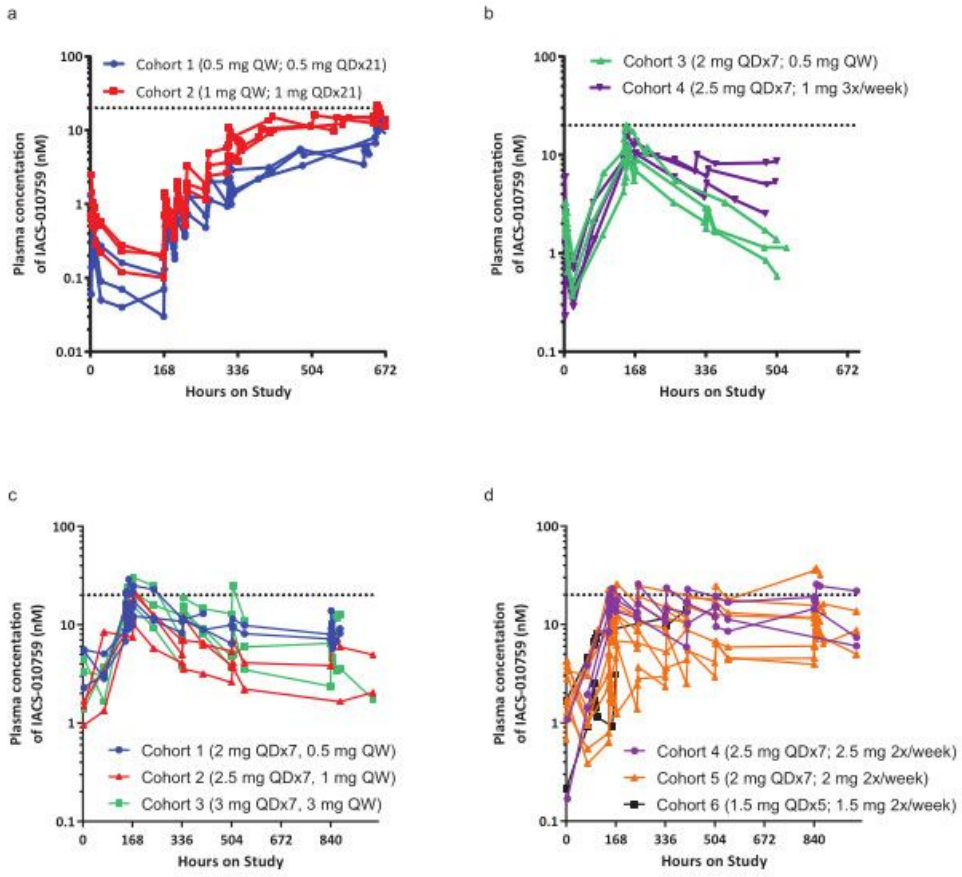

Figure 3

Figure 3

Pharmacokinetics of IACS-010759 in AML and Solid Tumor cohorts. Dosing regimens are detailed in Supplementary Table 1. **(a)** Plasma IACS-010759 concentrations in AML Cohort 1 (blue) and Cohort 2 (red). **(b)** Plasma IACS-010759 concentrations in AML Cohort 3 (green) and 4 (purple). **(c-d)** Plasma IACS-010759 concentrations (nM) over time in Solid Tumor (c) Cohorts 1-3 and (d) Cohorts 4-6. Each dot represents the mean plasma IACS-010759 concentration at one collection point for one cohort.

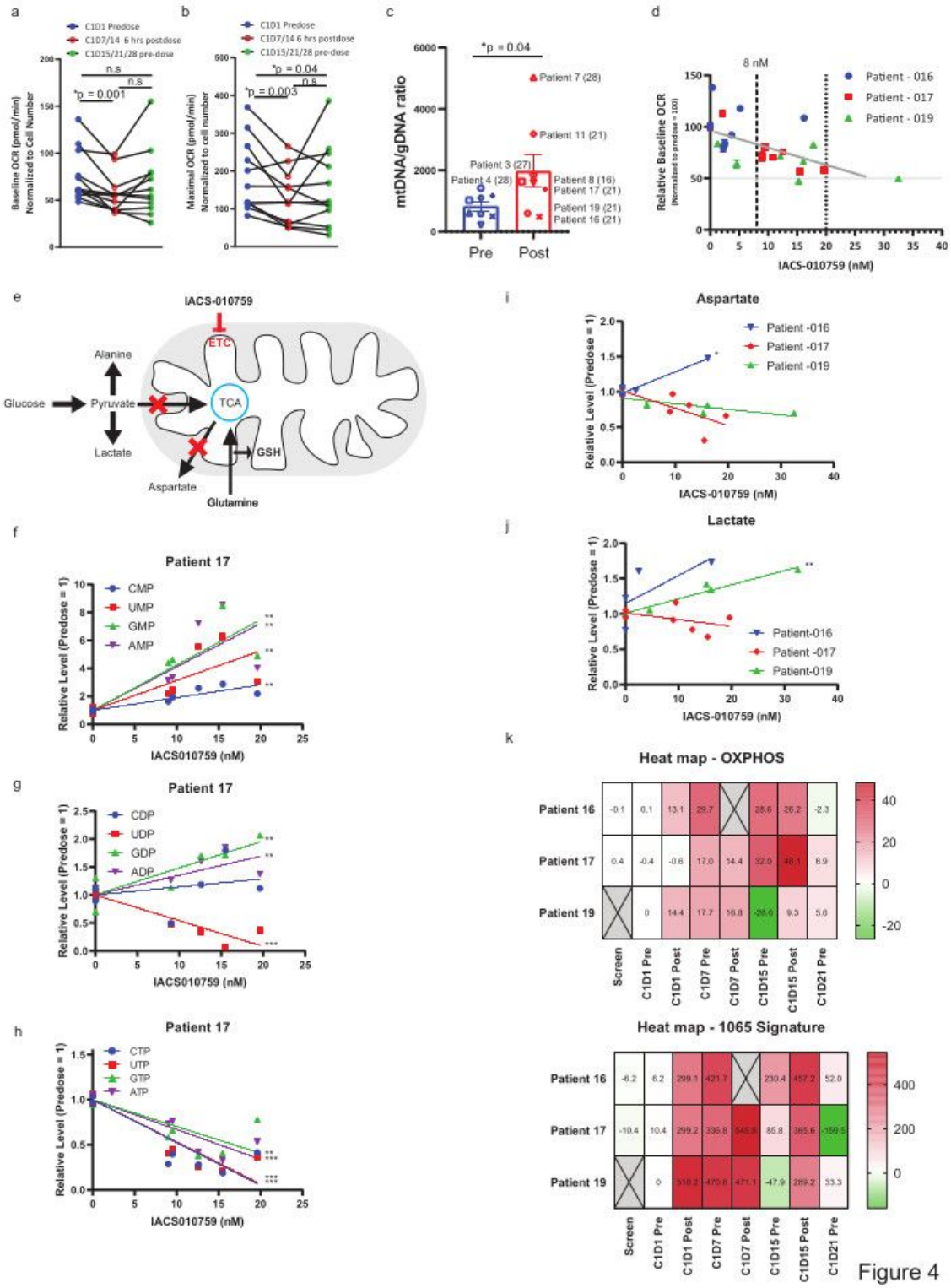

Figure 4

Figure 4

Evidence of target inhibition in AML blasts. (a-b) Change in (a) baseline and (b) maximal oxygen consumption rate (OCR) prior to dosing (C1D1), after one week of QD dosing (C1D7/C1D14), or extended dosing (C1D15/21/28). Differences were analyzed by paired Student's t-test.; n.s. = non-significant. **(c)**

Change in the ratio of mitochondrial DNA (mtDNA) to genomic DNA (gDNA) from AML blasts collected pre- and post-dose on Day 16/21/27/28. Difference from pre-dose levels were calculated with a paired Student's T-test. Post-treatment dots are labeled with patient number. Bars indicate mean ± SE. **(d)** Pharmacodynamics of IACS-010759 concentration on baseline OCR in AML blasts from AML Cohort 4 patients 16, 17, and 19. Grey line indicates expected modulation of baseline OCR by IACS-010759[15]. Dotted lines indicate the concentration of IACS-010759 associated with increased risk of peripheral neuropathy (8 nM) and target plasma concentration (20 nM). **(e)** Schematic depicting effects of IACS-010759 on oxidative metabolism and alternative fuel pathways. TCA = The tricarboxylic acid cycle; GSH = glutathione; ETC = electron transport chain. **(f-h)** Effect of IACS-010759 exposure on levels of (f) NMP, (g) NDP, and (h) NTP in AML blasts from AML Patient 17. Y-axis shows nucleotide levels respective to pre-dose levels. Differences from pre-trial levels analyzed by a linear regression; **p < 0.01, ***p < 0.001. **(i)** Effect of IACS-010759 on aspartate levels in AML blasts from AML Patients 16, 17, and 19. Y-axis shows aspartate levels relative to pre-dose levels. Differences from pre-trial levels analyzed by a linear regression; *p < 0.05. **(j)** Effect of IACS-010759 on levels of lactate in AML blasts from AML Patients 16, 17, and 19. Y-axis shows metabolite levels relative to pre-dose levels. Differences from pre-trial levels analyzed by a linear regression; **p < 0.01. **(k)** OXPHOS signature generated from (top) preclinical data published in Molina et al (2018) or from (bottom) 1065 mRNAs that were significantly modulated in AML blasts from AML Patients 16, 17, and 19.

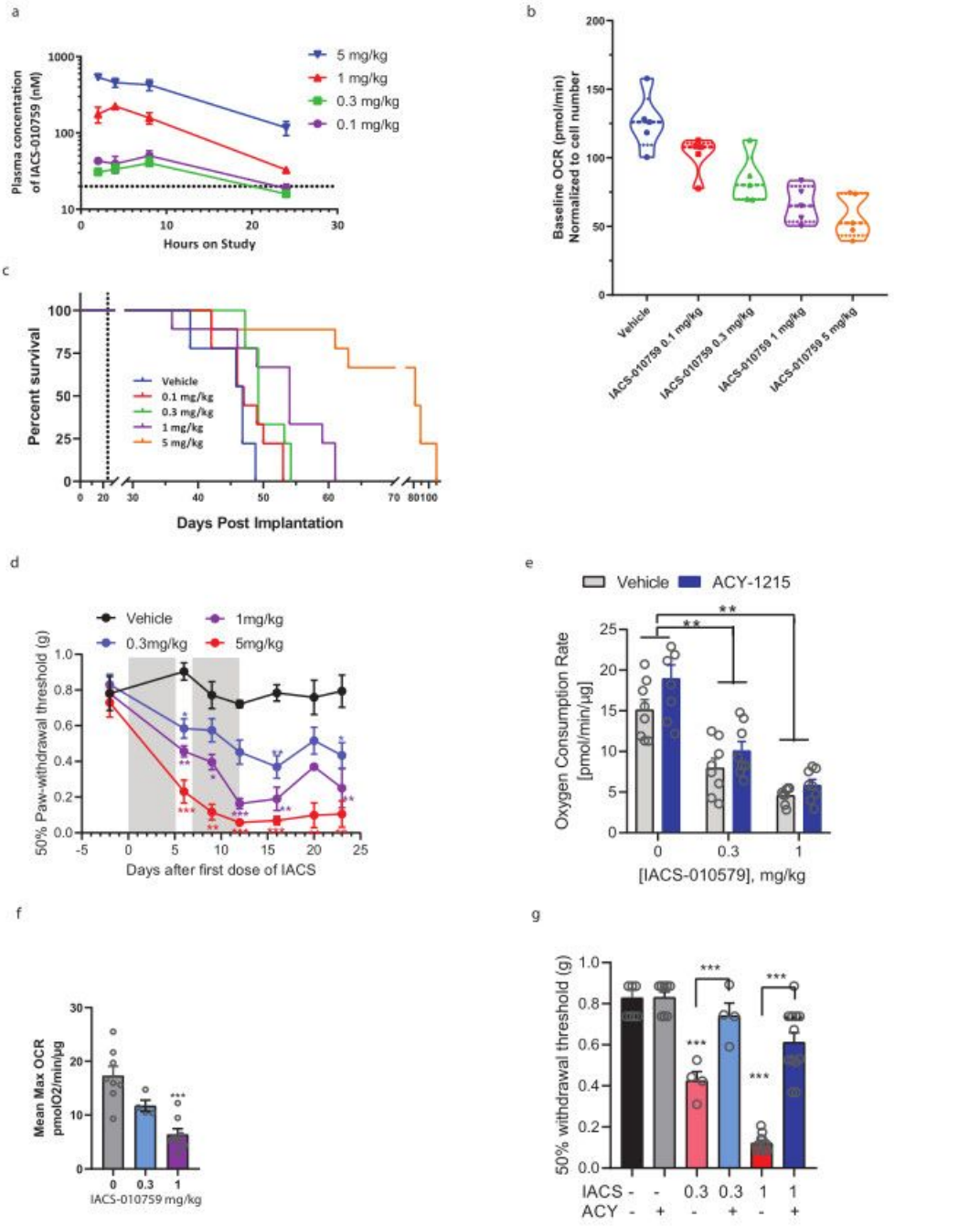

Figure 5

Figure 5

Reverse translational studies. (a) Change in plasma IACS-010759 concentrations in B6 mice treated with escalating doses of IACS-010759. Data show mean ± SE. **(b)** Violin plots show average baseline oxygen consumption rates (OCR) for mice treated with vehicle or escalating doses of IACS-010759. **(c)** Kaplan-Meier survival analysis of NSG/B6 mice treated with escalating doses of IACS-010759 or vehicle. Dotted line indicates first day of IACS-010759 treatment. **(d)** Mechanical sensitivity of hind paws of mice

(n=4/group) treated with two rounds of daily IACS-010759 or vehicle doses for 5 days on (grey) and 2 days off. Mechanical sensitivity was monitored using von Frey hairs at Day 6 after the first dose and then every 3-4 days for 24 days. Data are expressed as 50% withdrawal threshold, and shown as mean ± SE. Data analyzed with a two-way repeated measures ANOVA with a Dunnett's multiple comparison test; ***p<0.001, **p<0.01, *p<0.05 versus vehicle control. **(e)** OCR in DRG neurons was determined using Seahorse technology at 3-4 hours after the last dose of IACS-010759 or vehicle +/- ACY-1215. Differences analyzed by two-way ANOVA with Dunnett's multiple comparison test, **p< 0.01. Data represent mean ± SE; dots represent measurements from each mouse. **(f)** Mean maximal OCR of the dorsal root ganglion neurons (DRG) determined using Seahorse technology at 5 weeks after the last dose of IACS-010759 or vehicle in mice. Data analyzed by one-way ANOVA with Dunnett's multiple comparison test; ***p<0.01 vs vehicle control. Data represent mean ± SE; dots represent measurements from each mouse. **(g)** Mechanical sensitivity of hind paws of mice (n=4/group) treated with two rounds of daily IACS-010759 (0.3 mg/kg or 1 mg/kg) or vehicle +/- ACY-1215 for 5 days on (grey) and 2 days off. ACY-1215 or vehicle was administered 1 hour before IACS-010759 or vehicle. Mechanical sensitivity was monitored one day after completion of treatment. Data are expressed as 50% withdrawal threshold, and shown as mean ± SE. Differences from respective control groups were analyzed by two-way ANOVA with Sidak's multiple comparison test, ***p < 0.0001.

Supplementary Files

This is a list of supplementary files associated with this preprint. Click to download.

- Supplementarytables.pdf
- OXPHOSallEDfigs.pdf